Basal level of autophagy and MAP1LC3B-II as potential biomarkers for DHA-induced cytotoxicity in colorectal cancer cells

Helle Samdal[1], Malin A Sandmoe[1], Lene C Olsen[1,2], Elaf A H Jarallah[1], Therese S Høiem[1], Svanhild A Schønberg[1] and Caroline H H Pettersen[1,3,#]

1 Department of Clinical and Molecular Medicine, Faculty of Medicine and Health Sciences, Norwegian University of Science and Technology, NTNU, 7006 Trondheim, Norway

2 Bioinformatics core facility - BioCore, Norwegian University of Science and Technology, NTNU, 7006 Trondheim, Norway

3 Department of Surgery, St. Olavs Hospital, Trondheim University Hospital, N-7006 Trondheim

[#]Corresponding author. E-mail address: caroline.h.pettersen@ntnu.no

Caroline Hild Hakvåg Pettersen

Norwegian University of Science and Technology

Faculty of Medicine and Health Sciences

Department of Clinical and Molecular Medicine

Laboratoriesenteret 5th floor east,

Erling Skjalgssons gt 1

7006 Trondheim,

Norway

Phone: +47 72573539

URL: http://www.ntnu.edu/lbk/cancer

Running title: Basal autophagy and DHA cytotoxicity

Abbrevations

3-MA, 3-Methyladenine; ATCC, American Type Culture Collection; ATF4, Activating Transcription Factor 4; Bafa1, Bafilomycin A1; BHA, Butylated Hydroxyanisole; BHT, Butylated Hydroxytoluene; CHOP, TF C/EBP Homologous Protein; CRC, Colorectal Cancer; DCF, 5-(and-6)-Carboxy-2',7'-Dichlorodihydrofluoresceindiacetate, DHA, Docosahexaenoic Acid; DTT, Dithiothreitol; eIF2α, Eukaryotic Translation Initiation Factor 2 Alpha; ER, Endoplasmic Reticulum; EtOH, Ethanol; FACS, Fluorescence-Activated Cell Sorting; FBS, Fetal Bovine Serum; GO, Gene Ontology; HBSS, Hanks Balanced Salt Solution; HSP70, Heat Shock Protein 70, ISR, Integrated Stress Response; MAP1LC3B, Microtubule-Associated Protein 1 Light Chain 3β; NAC, N-Acetylcysteine; NFE2L2, Nuclear Factor, Erythroid Derived 2, Like 2; PARP1, poly(ADP-ribose) polymerase 1; PBS, Phosphate Buffered Saline; PERK, Pancreatic ER Kinase; PUFA, Polyunsaturated Fatty Acid; ROS, Reactive Oxygen Species; SQSTM1/p62, Sequestosome-1; TBS, Tris-Buffered Saline; TP53, Tumor Suppressor Protein 53; TRIB3, Tribbles pseudokinase 3; UPR, Unfolded Protein Response.

Databases

Protocol and data for gene expression experiments have been submitted to ArrayExpress with accession number E-MTAB-5750.

Keywords

Autophagy; colorectal cancer; DHA; MAP1LC3B; omega-3

Conflicts of interest

The authors report no conflicts of interest.

Abstract

The omega-3 fatty acid docosahexaenoic acid (DHA) is known as an anticancer agent. Colorectal cancer cells (CRCs) exhibit different sensitivity towards DHA, but the mechanisms involved are still unclear. Gene expression profiling of ten CRC cell lines demonstrated a correlation between the level of DHA sensitivity and different biological stress responses, like endoplasmic reticulum (ER) stress, oxidative stress and autophagy. The basal level of autophagy and MAP1LC3B-II protein correlated with DHA sensitivity in the cell lines studied. DHA induced oxidative stress, ER stress and autophagy in DHA sensitive DLD-1 cells, while the less sensitive LS411N cells were affected to a much lesser extent. Co-treatment with DHA and the autophagy inducer rapamycin reduced DHA sensitivity in DLD-1 and HCT-8 cells, while co-treatment with DHA and the autophagy inhibitors chloroquine and 3-methyladenine increased the DHA sensitivity in LS411N and LS513 cells. Differentially expressed genes correlating with DHA sensitivity and the level of autophagy demonstrated an overlap in biological pathways involved. Results indicate the basal level of autophagy and MAP1LC3B-II protein as potential biomarkers for DHA sensitivity in CRC cells.

Introduction

Colorectal cancer (CRC) is the third most common type of cancer worldwide, representing 10 % of the global cancer incidence according to the World Cancer Report (2014) [1]. About 1.4 million new cases were diagnosed in 2012, of which 65 % in highly developed countries [1]. Despite progress in early diagnosis and treatment (surgery, chemotherapy and radiotherapy), CRC caused approximately 770 000 deaths in 2015 [1, 2]. Lifestyle (alcohol, smoking) and diet (red/processed meat, fatty meals) are considered major risk factors [3]. However, increased physical activity and a diet rich in fruit, vegetables, fish and white meat seem to decrease the risk [4].

Although epidemiological studies have been inconclusive, several *in vitro*, *in vivo* and some clinical studies support the anticancer properties of the omega-3 polyunsaturated fatty acid (PUFA) docosahexaenoic acid (DHA, 22:6 n-3) [5-7], which may represent a nontoxic and safe way in the prevention and management of cancer. Moreover, omega-3 PUFAs have been reported to increase the effect of several anti-cancer drugs [8, 9]. A variety of mechanisms explaining the anti-carcinogenic properties of DHA have been reported, like oxidative stress, lipid peroxidation and eicosanoid synthesis (reviewed in [10]). We have previously shown that DHA induces endoplasmic reticulum (ER) stress, unfolded protein response (UPR) and growth arrest in several different colon cancer cells [11]. Our research group also found that one CRC cell line with low basal level of autophagy was more susceptible to treatment with DHA compared to another CRC cell line with higher basal autophagy level [6]. Both the UPR and autophagy signaling pathways are potential therapeutic targets for CRC. The ER is responsible for protein synthesis and folding, synthesis of lipids and sterols, and the maintenance of Ca^{2+} homeostasis in cells. Disturbances in any of these functions will induce ER stress and the UPR. As an immediate response to ER stress, PKR-like ER kinase (PERK) phosphorylates nuclear factor 2

(erythroid 2-like) (NFE2L2/Nrf2) and eukaryotic translation initiation factor 2 alpha (eIF2α), thereby triggering the antioxidant defense system and inhibiting protein synthesis, respectively. Despite attenuation of protein translation, activating transcription factor 4 (ATF4) is translationally upregulated to activate the integrated stress response (ISR), which includes target genes involved in resistance to oxidative stress, differentiation, metastasis, angiogenesis, amino acid synthesis, drug resistance, apoptosis and autophagy, and it is often found upregulated in tumors. However, not all genes regulated by ATF4 are associated with cell survival. If the ER stress is too severe, ATF4 induces pro-apoptotic genes, like TF C/EBP homologous protein (CHOP) [12, 13]. ATF4 also induces tribbles pseudokinase 3 (TRIB3), which often is found overexpressed in colon cancers and associated with poor prognosis [14].

Recent studies have suggested the eIF2α-ATF4 pathway as an important regulator of many autophagy genes [15, 16]. Autophagy is a highly regulated catabolic process activated in response to different kinds of stresses like damaged organelles, nutrient deprivation, reactive oxygen species (ROS), anticancer agents and protein aggregation [17]. Macroautophagy (hereafter referred to as autophagy) is initiated by the formation of an autophagosome that engulfs cellular components marked for degradation. The autophagosome fuses with a lysosome and the contents are degraded and recycled. Dysregulation of autophagy has been implicated in several diseases like cancer, neurodegenerative diseases, cardiovascular diseases, and infectious and metabolic diseases [17]. The role of autophagy in cancer growth and development is complicated, having both a possible pro-survival and a death-inducing role.

A commonly used marker to monitor autophagy is microtubule-associated protein 1, light chain 3 beta (MAP1LC3B/LC3B) [18]. MAP1LC3B is post-translationally modified to the lipidated form, MAP1LC3B-II, that attaches to the inner autophagosomal membrane where it remains until it is degraded after fusion with the lysosome [19]. Autophagy may be

selective, e.g. through binding of ubiquitinated proteins and organelles to the scaffold protein sequestosome 1 (SQSTM1) [20, 21].

The tumor suppressor protein p53 (TP53) is commonly found mutated in human cancers and contributes to disease progression and chemotherapy resistance. Mutant TP53 has increased stability, tends to accumulate in tumors and often exerts oncogenic properties by promoting angiogenesis, invasion, migration, survival and proliferation [22, 23]. TP53 also influences the autophagic process and may function both as a negative and positive regulator of autophagy depending on its subcellular localization. In the nucleus, TP53 increases autophagy by acting as a transcription factor trans-activating different autophagic inducers [24, 25]. Negative regulation occurs mainly via its cytoplasmic localization where even normal amounts of TP53 contribute to the suppression of autophagy, and the cytoplasmic level of TP53 has to be reduced to induce autophagy. Different cellular stresses known to trigger autophagy, including rapamycin, nutrient deprivation and toxins, influence the degradation of TP53 [24-27].

We here report that gene expression profiling of ten CRC cell lines demonstrated a correlation between DHA sensitivity and biological processes involved in the integrated stress response. Accordingly, ER stress and oxidative stress were induced in the DHA sensitive DLD-1 cells, but not in the less DHA sensitive LS411N cells. TP53 has previously been suggested to mediate DHA-induced growth inhibition in cancer cells. Our results showed that DHA reduced the protein level and the positive nuclear staining of TP53 in DLD-1 cells. DHA-induced cytotoxicity seemed to be TP53 independent, since knock down of TP53 did not affect DHA-sensitivity in these cells. However, we observed cytoplasmic aggregates positively stained for both TP53 and the autophagy marker MAP1LC3B-II in DLD-1 cells, indicating that autophagy was induced. Our results showed that DHA increased the autophagic flux in DLD-1, but not in LS411N cells. Also, DHA sensitivity correlated

with the basal levels of autophagy and MAP1LC3B-II protein in the ten different CRC cell lines. Extended gene expression analysis revealed that genes correlating with DHA sensitivity and basal autophagy level were enriched in biological processes such as oxidative stress, lipid metabolism and catabolism, and protein degradation. The results from this study indicate that the basal level of autophagy and MAP1LC3B-II protein may be used as potential biomarkers for DHA-sensitivity in CRC cells.

Results

Differences in DHA sensitivity correlate with differences in gene expression in CRC cell lines

Ten CRC cell lines, representing different clinically relevant CRC subtypes, were selected for gene expression analysis. Sensitivity towards DHA treatment (70 µM) was measured by cell counting and varied from ~50 % growth inhibition after 48 h for the most sensitive cell lines (DLD-1, SW480 and SW620), to almost no effect for the less sensitive cell lines (Caco-2, LS411N, LS174T and LS513) (Fig. 1A).

Gene expression analysis was performed for the same ten cell lines to search for pathways and mechanisms underlying the differences in DHA sensitivity. Data analysis yielded 339 probes significantly correlating with the level of DHA sensitivity (Fig. 1B). The statistical model fitted the data well, and the expression levels of the three most significant genes, transmembrane serine protease 4 (TMPRSS4), dopa decarboxylase (DDC) and A-kinase anchoring protein 12 (AKAP12), have all been linked to the pathological state or prognosis of CRC (Fig. 1C) [28-30]. Gene ontology (GO) enrichment analysis revealed probes representing genes belonging to several different biological pathways, like vesicle-mediated transport, unsaturated fatty acid metabolism, response to lipid, regulation of response to stress, regulation of phosphorylation, regulation of programmed cell death,

oxidation-reduction process, peroxisomes, ER membrane and Golgi apparatus (Fig. 1D and E). Examination of the gene list used for the GO analysis revealed several genes involved in regulation of ER stress, autophagy, lysosomal activity, protein metabolism and oxidative stress (Table 1). In regard to autophagy, it should be noted that GO term databases are not yet well enough annotated. Several genes with known functions in autophagy were therefore identified by manually inspection of gene lists. Among these was the DEP-domain containing mechanistic target of rapamycin (mTOR)-interacting protein (DEPTOR), which is an inhibitor of mTOR, a well-known regulator of autophagy. Hence, Table 1 is a selection of genes from the gene list that is known to be involved in the regulation of ER stress, oxidative stress and autophagy.

DHA induces oxidative stress and ER stress in DHA-sensitive DLD-1 cells

Based on the gene expression results and our previous findings suggesting that cytotoxic effects of DHA are associated with ER stress in CRC cell lines [11], we wanted to further examine the integrated stress response in the DHA-sensitive (DLD-1) and less sensitive (LS411N) cells (Fig. 2A). These cells were cultivated in the same growth media to exclude possible artifacts due to different culture conditions. Immunoblot analysis of total protein extracts from DLD-1 cells treated with DHA (70 μM) showed an upregulation of ER stress-related proteins, such as phosphorylated PERK and phosphorylated eIF2α at early time points (Fig. 2B), which is considered a hallmark of ER stress. This was not observed in LS411N cells (Fig. 2B). Phosphorylation of eIF2α leads to a general stop in translation, but increases the translation of certain proteins like activating transcription factor 4 (ATF4), which was found upregulated in DHA-treated DLD-1 cells at all indicated time points (Fig. 2B). ATF4 interacts with CHOP to induce TRIB3. Both CHOP and TRIB3 were found induced by DHA treatment in DLD-1 cells at time points indicated (Fig. 2B). CHOP and TRIB3 increased

slightly, although not significant, after 24 hours with DHA-treatment in LS411N cells (Fig. 2B). The results were confirmed by confocal imaging demonstrating nuclear upregulation of ATF4, CHOP and TRIB3 in DLD-1 cells after incubation with DHA (70 μM) at indicated time periods (Fig. 2C). The expression levels were further increased after treatment with DHA (105 μM). In LS411N cells, only TRIB3 was found to be slightly increased after treatment with DHA (105 μM) for 12 hours. Knock down of ATF4 using siRNA reduced the growth of control cells, but did not affect the growth-inhibitory effect of DHA (Fig. 2D). Prolonged ER stress may lead to activation of apoptosis, e.g through induction of CHOP [12]. However, examination of the protein poly(ADP-ribose) polymerase 1 (PARP1), which is known as a stress response modulator and is cleaved during apoptosis [31], showed that PARP1 was not cleaved after DHA treatment in DLD-1 cells (Fig. 2B).

Multiple lines of evidence indicate that ROS is involved in the DHA-mediated cytotoxicity in several cancer cells [32, 33]. To investigate the role of ROS in DHA-mediated growth inhibition, the effect of co-incubation with DHA (70 μM) and different antioxidants was examined. DHA-treated DLD-1 and LS411N cells were co-incubated with butylated hydroxyanisole (BHA, 50 μM), butylated hydroxytoluene (BHT, 50 μM), vitamin E (50 μM) and n-acetyl cysteine (NAC, 100 μM) for 24 and 48 hours before cell counting. BHT and vitamin E did not counteract the growth inhibitory effect of DHA in DLD-1 cells (Fig. 3B and C), while BHA further increased the growth inhibitory effect of DHA (Fig. 3A). However, NAC, a potent ROS scavenger, counteracted the DHA-induced growth inhibition in DLD-1 cells by about 16% (Fig. 4A).

The mitochondrial superoxide level was detected by flow cytometry using the fluorescent MitoSox probe. Results indicated a high increase in mitochondrial superoxide in DLD-1 cells after DHA (70 μM) treatment, which increased further after co-incubation with

DHA and NAC (Fig. 4B). Only a slight increase in mitochondrial superoxide level was observed in LS411N cells after DHA (70 µM) treatment (Fig. 4B).

The fluorescent DCF probe was used to measure cellular ROS levels in DLD-1 and LS411N cells by flow cytometry (Fig. 4C). Results clearly demonstrated an increased cellular ROS level in DLD-1 cells after 6 and 24 hours incubation with DHA (70 µM) (Fig. 4C). The increased ROS level in DLD-1 cells was reduced when co-incubating the cells with DHA and NAC (100 µM) (Fig. 4C). The cellular ROS level in LS411N cells were not affected by the same treatment (Fig. 4C).

Immunoblotting and confocal imaging indicated an induction of the antioxidant regulator NFE2L2 in DLD-1 cells after DHA (70 µM) treatment, which indicates induction of oxidative stress (Fig. 2B and C). An induction of NFE2L2 was detected in LS411N cells upon DHA treatment, however to a lesser extent compared to DLD-1 cells (Fig. 2B and C, Fig. 4D).

Accumulation of unfolded proteins in the ER lumen may trigger the production of ROS, which induces the transcription of genes involved in the anti-oxidant defense through the PERK-mediated phosphorylation of NFE2L2 [34]. Therefore, co-treatment with DHA and NAC was performed to investigate whether it would affect the expression level of ER stress proteins. Indeed, co-treatment with NAC clearly reduced the DHA-mediated upregulation of ATF4, SQSTM1 and NFE2L2 (Fig. 4D). The same trend was observed although to a lesser extent in LS411N cells (Fig. 4D).

DHA causes mutant TP53 to decrease and form aggregates in DLD-1 cells

Previous studies have found DHA-mediated growth inhibition to be TP53 dependent in cancer cells harboring wt TP53 [35, 36], while others have found TP53 independent pathways induced by DHA in cancer cells with mutant TP53 gene and no detectable protein

[32]. When present, TP53 seems to play a central role in DHA-mediated cytotoxicity [37]. Since there are several variants of mutant TP53 present in different types of cancers, the role of TP53 in DHA-mediated growth inhibition probably changes with cell type and mutational status. DLD-1 cells harbor a mutant TP53 (p.S241F) with a high level of detectable TP53 protein, while LS411N cells have a mutated TP53 gene (p.Y126) which gives a truncated non-detectable TP53 protein [38, 39]. Results from immunoblot analysis showed that the protein level of TP53 in DLD-1 cells decreased after 12 and 24 hours incubation with DHA (70 µM), and this reduction was counteracted by NAC (Fig. 5A).

Confocal imaging indicated that TP53 was mainly localized in nucleus in DLD-1 control cells (Fig. 5B). DHA treatment reduced the positive nuclear staining of TP53 and induced cytoplasmic aggregates positively stained for TP53 (Fig. 5B). Co-incubation with DHA and NAC increased the number of nuclei positively stained for TP53 compared with DHA-treated cells, 25% of DHA-treated DLD-1 cells had positive staining for TP53 in the nuclei, compared to 42% after co-treatment with NAC (Fig. 5B).

TP53 is known as an autophagy regulator [24] and we wanted to investigate the localization of cytoplasmic TP53 aggregates relative to the localization of MAP1LC3B in DLD-1 cells after DHA (70µM) supplementation. Fig. 5B indicates a co-localization of TP53 and MAP1LC3B aggregates in DHA-treated DLD-1 cells. Treatment with bafilomycin A1 (BafA1), an autophagy inhibitor, did not cause TP53 aggregation. Also, bafA1 alone or in combination with NAC did not affect the formation of DHA-induced TP53 aggregates. SiRNA mediated knock down of TP53 reduced the growth of control cells by approximately 60 %, but did not affect the DHA-induced growth inhibition in DLD-1 cells (Fig. 5C).

DHA increases the autophagic flux in DLD-1 cells

ER- and oxidative stress are known to be inducers of autophagy (reiewed in [40]). To investigate the effect of DHA on the level of autophagy in DLD-1 and LS411N cells, the amount of autophagic vacuoles were measured using the fluorescent autophagic marker Cyto-ID. The level of autophagic flux was determined by comparing cells co-incubated with DHA and BafA1with cells supplemented with BafA1 alone. MAP1LC3B is necessary for the elongation of the autophagosome. The amount of the lipidated form, MAP1LC3B-II, correlates with the amount of autophagosomes and is commonly used as an indicator of autophagosome formation. Our results show that DHA treatment induces autophagic flux in DLD-1 cells, but not in LS411N cells (Fig.6A, B and C). Confocal imaging indicated an increase in both SQSMT1 and MAP1LC3B upon DHA treatment for 12 and 24 hours in DLD-1 cells. Similarly, when co-incubating with BafA1 and DHA, an increased induction of SQSTM1 and MAP1LC3B was observed in comparison to BafA1 alone (Fig. 6A). The protein level of SQSTM1 and MAP1LC3B seems to be higher in LS411N cells compared to DLD-1 cells, but the level of these proteins was not affected by any of the treatments (Fig. 6A). Immunoblot analysis of both cell lines were performed after treatment with DHA (70 μM), with or without BafA1 (100 nM). Results demonstrated an increased autophagic flux in DLD-1 cells in response to DHA incubation (12 and 24 hours), while the level of MAP1LC3B-II was reduced in LS411N cells after the same treatment (Fig. 6B). The increased level of SQSTM1 in both cell lines after DHA-treatment is most likely due to increased cellular ROS, since NAC counteracts this effect (Fig. 4D and 6B). Flow cytometry using the Cyto-ID probe to stain autophagic vacuoles also showed an increased level of autophagy upon DHA-treatment in DLD-1 cells (Fig. 6C). NAC reduced the autophagic flux induced by DHA in DLD-1 cells, as demonstrated by confocal imaging, immunoblotting and the Cyto-ID assay (Fig.6A, B and C).

DHA sensitivity correlates with basal level of autophagy and MAP1LC3B-II in CRC cells

Previous results from our group suggest that the basal level of autophagy might be important for DHA sensitivity of human CRC cell lines. The basal level of autophagy in DLD-1 and LS411N cells was investigated using the Cyto-ID assay. Results indicated that the less DHA-sensitive LS411N cells had a much higher (3.2 fold) level of basal autophagy compared to DLD-1 cells (Fig. 6D and Fig. 7A). To elaborate these findings, the basal level of autophagy was measured in a panel of ten different CRC cell lines differing in DHA sensitivity. The results demonstrated that the basal level of autophagy varied significantly between the different cell lines (Fig. 7A). Interestingly, the degree of DHA-sensitivity between the cell lines correlated with the level of basal autophagy (correlation coefficient 0.93) (Fig. 7C) and the basal level of MAP1LC3B-II protein (correlation coefficient 0.92) (Fig. 7B and D). The basal level of MAP1LC3B-II protein also correlated with the basal level of autophagy (correlation coefficient 0.93) (Fig. 7E). To confirm the correlation between the level of basal autophagy and DHA sensitivity, the DHA-sensitive DLD-1 and HCT-8 cells were incubated with DHA (70 µM) and rapamycin (50 nM), or a combination of these. Rapamycin, which is an autophagy inducer, reduced the DHA-induced growth inhibition with ~30 % and 15 % in DLD-1 and HCT-8 cells, respectively (Fig. 7F). The protein level of MAP1LC3B-II was increased by rapamycin, and to an even higher level after co-treatment with rapamycin and DHA (Fig. 7F). The less DHA-sensitive LS411N and LS513 cells were incubated with DHA (140 µM), chloroquine (40 and 80 µM), 3-MA (3 mM), or a combination of DHA and one of these autophagy inhibitors. The results demonstrate that inhibition of autophagy significantly increased the DHA sensitivity in these two cell lines (Fig. 7G and H). A higher concentration of DHA (140 µM) was used for LS411N and LS513 cells in order to detect the effect on cell number, while 70 µM DHA was used for the immunoblots. The protein level of MAP1LC3B-II was increased by treatment with either chloroquine or 3-MA in these cells; after co-

treatment with chloroquine/3-MA and DHA (70 µM), the protein level of MAP1LC3B-II decreased significantly (Fig. 7G and H). These results indicate that DHA induces autophagic flux in DHA-sensitive cell lines (DLD-1 and HCT-8), while the autophagic flux is decreased by DHA in less sensitive cell lines (LS411N and LS513). The autophagy level in these cells, measured by flow cytometry and the fluorescent Cyto ID probe, was affected in line with these results after the same treatment (Fig. 7I).

Gene expression profile correlates with both DHA sensitivity and basal autophagy level

Gene expression data was analyzed for correlation with scaled basal autophagy levels, revealing 1268 probes to be significantly correlated (Fig. 8A; adjusted p value 0.05). Of these, 309 also correlated with scaled DHA sensitivity levels. Although autophagy and sensitivity measurements were highly correlated between the cell lines, they still differed. Therefore, we investigated whether differences between autophagy and DHA sensitivity could be explained by certain genes. Accounting for residuals in the analysis, extended the list of significantly correlating probes for both DHA sensitivity and autophagy (Fig. 8B; 637 and 1345 probes, respectively). The expression of 608 probes correlated with both in this analysis. GO term enrichment analysis clearly shows an overlap in the represented biological processes and cellular compartment between probes correlating with DHA sensitivity and those correlating with the basal autophagy level (Fig. 8C and D). Among overlapping GO terms for biological process were “lipid homeostasis”, “oxidation-reduction process”, “cellular lipid catabolic process” and “unsaturated fatty acid metabolic process”. Overlapping GO terms for cellular compartment were e.g. “golgi apparatus”, “endoplasmic reticulum membrane”, “peroxisome”, “endosome” and “lysosome”. No significantly enriched terms were found for the probes representing residuals in the linear model, i.e. the probes that can better be described by one process and not the other.

Autophagy was not among the enriched terms for significant probes, with an adjusted p-value of 1. Only 21 probes belonging to the GO category for autophagy (GO:0006914) and its children significantly correlated with scaled basal autophagy or DHA sensitivity levels, e.g. the probes for ATP1B1 and USP13 (Fig. 8E). However, we found genes known to be involved in the regulation of autophagy with significant correlation that were both listed and not listed in the GO category for autophagy, including AKT3 and DEPTOR (Fig. 8E).

Discussion

Marine omega-3 fatty acids, such as DHA, have been shown to have anticancer properties. We and others have studied the mechanisms behind this anticancer effect mainly based on observations from a few cancer cell lines. The fact that some cancer cells are sensitive towards DHA, while others are not, needs special attention. The relevance of cancer cell lines as preclinical models is often questioned, since *in vitro* culturing fails to maintain the natural microenvironment of cells. Also, cancer patients often have heterogeneous genetic features implying that a large number of cell lines needs to be analyzed in order to mimic the molecular heterogeneity in patients. Medico *et al*. (2015) have analyzed a collection of 151 CRC cell lines by mutational and transcriptional profiling, and discovered that the molecular subtypes of CRC in patients are maintained in the cell lines [41]. They conclude that genetic and pharmacological profiling of CRC cell lines can be used in search for clinically relevant biomarkers for targeted treatment response.

In search for a potential biomarker for DHA-induced cytotoxicity, we selected ten CRC cell lines representing 5 clinically relevant CRC subtypes [42] that differed in sensitivity to DHA treatment (Fig. 1A). Gene expression profiling indicated a correlation between the expression of genes involved in the regulation of different biological processes, like response to autophagy, ER stress (UPR) and oxidative stress, and DHA sensitivity in the

ten cell lines (Fig. 1E and Table 1). These biological processes are part of the integrated stress response and were found to be induced by DHA treatment in DHA sensitive DLD-1 cells (Fig. 2B and C, Fig.4A, Fig. 6A and B), confirming previous results by our research group and others [6, 11, 37]. Interestingly, co-treatment of the DHA sensitive DLD-1 cells with the antioxidant NAC reduced the DHA-induced growth inhibition, cellular oxidative stress and protein level of NFE2L2 and ATF4 (Fig. 4A, C and D). These results suggest an interconnection between the ER- and oxidative stress signaling pathways in response to DHA treatment in this cell line.

The tumor suppressor protein TP53 is known to be mutated in over 40 % of colorectal tumors [43]. The TP53 status is different between DLD-1 and LS411N cells; DLD-1 cells express a mutated form of TP53 protein, while the TP53 mutation in LS411N cells results in no TP53 expression. It has previously been shown that DHA treatment of cancer cells initially escalate TP53 protein level, before it decreases [37, 44], which is in accordance with our results (Fig. 5A). However, our results also demonstrate that nuclei positive for TP53 decreases and aggregates are formed in the cytoplasm after DHA treatment. This effect was partly counteracted by NAC (Fig. 5B). Cytoplasmic aggregation of mutant TP53 in cancer cells followed by induction of heat shock protein 70 (HSP70) has previously been demonstrated [45]. HSP70 is commonly induced by ER stress, which corresponds with our previous finding in DHA sensitive SW620 colon cancer cells [6].

ER- and oxidative stress, as well as several other stressful conditions, affect the expression of TP53 and the level of autophagy (reviewed in [40]). TP53 is known to affect the autophagic process both as positive and negative regulator, depending on its localization. In the nucleus, TP53 activates autophagy-stimulating genes, while cytoplasmic TP53 inhibits autophagy (reviewed in [40]). When co-incubating the DHA sensitive DLD-1 cells with antibodies for both TP53 and the autophagy marker protein MAP1LC3B, both aggregated in

the cytoplasm upon DHA treatment, suggesting that MAP1LC3B- and TP53 aggregates co-localize upon DHA treatment (Fig. 5B). Interestingly, co-treatment of DLD-1 cells with DHA and NAC partly counteracted the decrease in TP53 protein level (Fig. 5A). Knock down of TP53 strongly reduced growth of the DLD-1 control cells, however failed to influence the DHA sensitivity, suggesting that the expression of TP53 is important for the cell growth, although it probably does not play an important role in the DHA mediated growth inhibition in DLD-1 cells (Fig. 5C). These results are in accordance with findings from Shin et al. (2013), who demonstrated that DHA reduced cell viability independent of TP53 status [37].

Our results clearly demonstrate that DHA treatment enhanced the autophagic flux in the DHA sensitive DLD-1 cells (Fig. 6A, B and C). The autophagic flux was subsequently reduced upon treatment with the antioxidant NAC, which is in accordance with previous studies [6, 37, 44, 46]. Further elucidation of the role of autophagy related to DHA sensitivity in the ten human CRC cell lines revealed that these cell lines have significantly different basal level of autophagy (Fig. 7A). Previous results from our group indicated the importance of the basal level of autophagy in two colorectal cancer cell lines differing in DHA sensitivity, which is clearly supported by the more comprehensive experiments presented here. Correlation analysis provided a strong correlation between basal autophagy level and DHA sensitivity (Fig. 7C). Other studies have shown that the autophagy level in cells may be important for their response/resistance to different chemotherapeutic agents (reviewed in [47]). Autophagy may have a dual role in its interaction with anticancer drugs. Induction of autophagy-mediated cell death may enhance the anticancer drug efficiency in some cancers [48], although it is more common that autophagy increases cancer cell survival by contributing to development of drug resistance. Autophagy-mediated drug resistance is probably a cell-protective mechanism against the cytotoxic effect of anticancer drugs, promoting cancer cell survival. Several studies have demonstrated that inhibition of

autophagy enhances the effect of chemotherapy in colorectal cancer [49-51], which makes it a promising therapeutic target to overcome drug resistance and thereby increasing the effect of different anticancer therapies.

Induction of autophagy by rapamycin reduced DHA sensitivity in DLD-1 and HCT-8 cells (Fig. 7F), while autophagy inhibitors, chloroquine and 3-MA, increased the DHA sensitivity of LS411N and LS513 cells (Fig. 7G and H). The significant effect of 3-MA on DHA sensitivity needs to be further examined to find the underlying mechanism; however, some studies have indicated the relevance of the PI3K/AKT/mTOR signaling pathway in omega-3 fatty acid-mediated growth inhibition of cancer cells [37, 46].

The protein level of the lipidated form of MAP1LC3B (MAP1LC3B-II), a commonly used marker to monitor autophagy, was found to correlate with the degree of DHA sensitivity (Fig. 7B and D). Hence, the MAP1LC3B-II protein level was lower in the most DHA sensitive cell lines, which is in accordance with our previous results [6]. Adams *et al*. (2016) explored the prognostic relevance of MAP1LC3B and SQSTM1 in esophageal adenocarcinomas (EAC) and demonstrated that low MAP1LC3B and SQSTM1 protein levels correlated with worse outcome and more aggressive tumors in a cohort of patients with EAC [52]. In line with this, patients with tumors with low MAP1LC3B-II levels could potentially benefit from an alternative treatment strategy with omega-3 fatty acids in combination with conventional cancer treatment. Intratumor heterogenic expression patterns of proteins may occur. However, Adams *et al*. (2016) found that most of the studied EACs had homogenous MAP1LC3B staining patterns across tumors [52], and Niklaus *et al*. (2017) found that primary resected colon cancer tissue stained for MAP1LC3B did not show significant intratumoral heterogeneity [53].

In cancer, autophagy has dual roles and can act as both a tumor promoter and a tumor suppressor. Autophagy protects against the development and progression of cancers by

removing damaged organelles, ROS and protein aggregates, while promoting carcinogenesis by providing increased amounts of available nutrients, enhancing drug resistance and inhibiting cell death [54]. Autophagy is known to be influenced by the ingredients of the growth media, e.g. the amino acid content. By using the same culture media for the cell lines DLD-1, LS411N, HCT-8 and LS513, the potential influence of different media constituents on the autophagy process was excluded. Accordingly, natural variance in basal autophagy and MAP1LC3B-II protein between cancer cells seems likely. However, this has to be confirmed in tumor samples from a patient cohort.

Omega-3 fatty acids have been shown to improve the effect of different chemotherapeutic drugs (reviewed by [8, 55]). The understanding of how genetic differences in CRC affect nutrient metabolism is a highly relevant nutrigenomic approach that may translate into recognition of new biomarkers potentially improving CRC treatment regimens. Next generation sequencing of CRC cell lines and patient tumors could help us to further explore the potential application of DHA in personalized treatment/diets for CRC patients, in combination with conventional cancer treatment.

Materials and methods

Cell lines, culture conditions and reagents

The ten human CRC cell lines DLD-1, LS411N, LS513, HCT8, Lovo, LS174T, HT29, Caco-2, SW620 and SW480 were obtained from the American Type Culture Collection (ATCC, Rockville, MD, USA). DLD-1, LS411N, LS513 and HCT8 cells were grown in RPMI 1640 medium (Gibco, England, A10491-01), supplemented with 10 % fetal bovine serum (FBS, Gibco, 10270-098) and gentamicin (Gibco, 15710049). LS174T and Caco-2 cells were grown in Eagle Minimum Essential Medium (Sigma, St. Louis, MO, USA, M5650), supplemented with gentamicin and FBS (10 or 20 %, respectively). Lovo cells were grown in Ham's F-12K (Kaighn's) medium (Gibco, 21127-022). HT29 cells were grown in Mc Coy`s 5A medium (Lonza, Basel, Switzerland, BE12-688F), and SW480 and SW620 cells were grown in Leibovitz`s L-15 medium (Lonza, BE12-700F). The following treatments were used: docosahexaenoic acid (DHA, Cayman Chemical, Ann Arbor, MI, USA, 90310), docosahexaenoic acid (DHA, Sigma, D2534), n-acetyl cysteine (NAC, Sigma, A9165), butylated hydroxyanisole (BHA, Sigma, B1253), butylated hydroxytoluene (BHT, Sigma, B1378), vitamin E (± - α-tocopherol, Sigma, T325), bafilomycin A1 (BafA1, Sigma, B1793), Hanks Balanced Salt Solution (HBSS, Sigma, H8264), rapamycin and chloroquine (part of the Cyto-ID detection kit, Enzo Life Sciences, Farmingdale, NY, USA, ENZ-51031), 3-Methyladenine (3-MA, Sigma, M9281) and ethanol (EtOH, VWR chemicals, Radnor, PA, USA, 20821.310). The cells were incubated at 37°C, 5 % CO_2 and humidified atmosphere. Cells were transfected using Lipofectamine® RNAiMax transfection reagent (Invitrogen, Carlsbad, CA, USA 13778075), ATF4 siRNA (Qiagen, Hilden, Germany, SI03019345), p53 siRNA no.3 (target sequence: 5′-CAGAGTGCATTGTGAGGGTTA-3′, Qiagen, SI00011655), AllStars Negative control (Qiagen, 1027280), Opti-MEM® I (Gibco, 31985070) and AllStars Hs Cell Death siRNA (Qiagen, 1027298).

Cell treatment and assessment of growth inhibition

The effect of DHA and different antioxidants were investigated by cell counting. 24 hours after seeding, DHA (70 μM), BHA (50 μM), BHT (50 μM), vitamin E (50 μM), NAC (1 mM), BafA1 (0.1 μM), 3-MA (3 mM), chloroquine (40 and 80 μM), rapamycin (50 nM), EtOH (vehicle) or HBSS were added to pre-heated growth medium to final concentrations as described. Cells were treated for indicated time periods before trypsination and resuspension in growth medium. The effect of the different treatments was assessed by cell counting using Moxi z mini automated cell counter (ORFLO Technologies, Ketchum, ID, USA).

Antibodies and immunoblot analysis

Cells were harvested at different time points after treatment, and total protein was isolated. The medium was removed and the cells were washed twice with ice cold PBS, before scraping in cold PBS. The cells were lysed using a buffer containing UREA (8M) (Merck Millipore, Darmstadt, Germany, 1084870500), Triton-X100 (0, 5 %) (Sigma, T8787), DTT (100 nM), Complete® protease inhibitor (Roche, Mannheim, Germany, 1187350001) and phosphatase inhibitor cocktail II and III (Sigma, P5726 and P0044). The concentration of the proteins was determined using the Bio-Rad assay (Bio-Rad, Hercules, CA, USA, 500-0006). Proteins were separated by Western blotting (SDS-polyacrylamide electrophoresis) using NuPAGE® NOVEX®10 % or 12 % Bis-Tris Gels (Invitrogen, NP0302BOX or NP0342BOX) and transferred on to an Immobilion Transfer Membrane (Merck Milipore). Membranes were blocked for 1 hour using Odyssey blocking buffer (Li-cor Biosciences, Lincoln, NE, USA, #27-40000). Primary antibodies were diluted in Odyssey blocking buffer and incubated with the membrane on a roller for 1 hour in room temperature. After washing in Tris-buffered saline (TBS) with tween, secondary antibodies were diluted in Odyssey blocking buffer and incubated with the membrane in a dark room on a roller for 1 hour.

Membranes were washed with TBS and the Odyssey Imaging System (Li-cor Biosciences) was used to visualize the proteins on the membrane. Primary antibodies used: PERK (Abcam, Cambridge, England, ab105929), phosphorylated PERK (Santa Cruz Biotechnology, Dallas, TX, USA, Sc-32577), eIF2α (Abcam, ab5369), phosphorylated eIF2α (Cell Signaling Technologies, Danvers, MA, USA, D9G8, 3398), ATF4 (Cell Signaling Technologies, D4B8, 11815S), CHOP (Fisher Scientific, Hampton, NH, USA, MA1-250, 11554842), TRIB3 (Sigma, HPA015272), NFE2L2 (Nrf2, Cell Signaling Technologies, D1Z9C, 12721), TP53 (DAKO/Agilent, Santa Clara, CA, USA, M700129-2, DO-7), MAP1LC3B (3868, D11, Cell Signaling Technologies), SQSTM1 (Progen Biotechnik, Heidelberg, Germany, GP-62-C), PARP-1 (Santa Cruz, F-2, sc-8007), COX IV (Abcam, ab33985) and β-actin (Abcam, AC-15, ab6276). Secondary antibodies used for immunoblotting were obtained from LI-COR (IRDye 680RD and IRDye 800RD), while secondary antibodies used for immunofluorescent staining were from Life Technologies (Carlsbad, CA, USA, Alexa conjugates, A11008 and A11017). CoxIV or β-actin was used as loading controls.

For detection of autophagic flux, control cells and cells treated with DHA (70 μM) and/or BafA1 (100 nM), rapamycin (50 nM), chloroquine (40/80 μM) and 3-methyladenine (3mM) were analyzed.

Measurement of intracellular ROS

The fluorescent based ROS detection kit Image-iT™ LIVE Green Reactive Oxygen Species Detection Kit (Life Technologies, C6827), was used to measure the cellular level of ROS, and MitoSOX ™ (Life Technologies, M36008) was used to measure the cellular level of mitochondrial superoxide, according to the supplier's instructions. DLD-1 and LS411N cells were treated with DHA (70 μM) and/or NAC (1 mM) for 6 and 24 hours and co-incubated

with DCF (0.3 μM) or MitoSOX ™ (5 μM) for 30 min before measuring intracellular ROS and mitochondrial superoxide, respectively. Fluorescence was measured using a BD FACS Canto flow cytometer (BD Biosciences, Franklin Lakes, NJ, USA).

Detection of autophagy levels by flow cytometry

Both changes in autophagic flux in response to DHA treatment in DLD-1, HCT-8, LS513 and LS411N cells and the basal level of autophagy of ten different human CRC cell lines were measured using the Cyto-ID autophagy detection kit (Enzo Life Sciences, ENZ-51031-K200) according to the manufacturer's instructions. The cells were given various treatments, trypsinated and stained with Cyto-ID detection agent for 30 min. The intensity of fluorescence per cell was determined using a BD FACS Canto flow cytometer, and analyzed using the FCS Express 5 Plus Research Edition (Denovo software). The optical readings from Cyto-ID experiments were log2 transformed before performing Pearson correlation analysis using Microsoft excel.

Immunostaining and confocal imaging

DLD-1 and LS411N cells were seeded in chamber slides (Nunc^{TM}, 734-2062) and received appropriate treatments as specified for indicated time periods. The cells were fixed using 4 % paraformaldehyde (Alfa Aesar, Haverhill, MA, USA, 43368.9M) before staining with primary antibodies and appropriate fluorescently labeled secondary antibodies for visualization. DRAQ 5 (5 μM) (BioStatus ltd, Loughborough, England, DR50200) was used as nuclear DNA marker. An Axiovert200 microscope equipped with a 63×1.2W objective and the confocal module LSM510 META (Carl Zeiss) were used to visualize the immunostaining. Images were processed using the LSM software (Carl Zeiss) and mounted using Canvas 15 (ACD Systems).

siRNA-mediated knockdown of ATF4 and TP53

DLD-1 cells were seeded and transfected using ATF4 (Qiagen, SI03019345, 20 nM) and TP53 (Qiagen, SI00011655, 10 nM) specific siRNAs, negative control siRNA oligo, and Lipofectamine RNAiMax transfection buffer (Invitrogen, 13778075) for 48 h, following the manufacturer's protocol (Fischer Scientific). Cells were then trypsinized, seeded and cultivated for 24 hours before supplemented with vehicle or DHA. Proteins were isolated and cells were counted after 24 and 48 hours incubation.

Gene expression profiling

Untreated cells were harvested by scraping in ice-cold PBS 48 hours after seeding. RNA was isolated using the High Pure Isolation Kit (#11828665001, Roche) before quantification and quality control using NanoDrop and BioAnalyzer. Expression profiling was performed in duplicate experiments using the Human Genome U133 Plus 2.0 array from Affymetrix, (Santa Clara, CA, USA) following standard procedures. Protocol and data have been submitted to ArrayExpress with accession number E-MTAB-5750.

Gene expression data analysis

All data analysis was conducted in R unless otherwise specified (http://r-project.org). We analyzed the microarray data using the Affy and Limma packages from BioConductor [56, 57]. The raw expression values (CEL files) were adjusted using the "expresso" function with "rma" background correction, quantile normalization, and "medianpolish" summarization. The normalized data was fit to a linear model using scaled DHA sensitivity growth restriction values in Limma with the duplicateCorrelation function to account for the replicates. Pearson correlation value between the expression values for each probe and the scaled DHA-sensitivity growth inhibition values was calculated. The data was fit to a linear model using

scaled Cyto-ID autophagy values in the same manner. Extended Limma analyses were performed with residuals from autophagy as a third coefficient for the sensitivity regression, and the residuals from sensitivity as a third coefficient for autophagy regression. Resulting p-values were adjusted using the Benjamini-Hochberg method, and a threshold of 0.05 for selection of genes fitting the models. The gProfileR tool [58] was used to analyze for overrepresented GO terms, and the "analytical" setting was used for multiple testing correction. The odds ratio for each term was calculated using the Fisher's exact test. Only terms that contained a maximum of 1500 genes were included. Redundant terms were eliminated using the minimal set function in the ontologyIndex package [59]. Where specified, we ran an additional filter to select term names containing the following key words; "lipid", "oxidative", "oxidation", "vesicle", "stress", "protein metabolic", "autophagy", "protein catabolic", "unfolded protein" and "fatty acid".

Acknowledgments

We appreciate the technical assistance by Grete Klippenvåg Pettersen and Almaz Nigatu Tesfahun. Gene expression analysis was performed at the Genomics Core Facility (GCF), Norwegian University of Science and Technology (NTNU). This work was supported by grants from the Joint Research Committee between St. Olavs Hospital and the Faculty of Medicine and Health Sciences, NTNU (FFU), The Faculty of Medicine and Health Sciences, NTNU, the Cancer Research Fund at St. Olavs Hospital, the Central Norway Regional Health Authority and the Research Council of Norway through "Småforsk" grant.

Author contributions

SAS, CHHP and **HS** designed the study and interpreted the results. **HS, MAS, TSH, EAHJ** and **CHHP** performed the experiments. **LCO** analyzed the gene expression data. All authors contributed to the writing of the manuscript and have approved the final version.

References

1. World Cancer Reserach Fund International (2015) Colorectal cancer statistics. http://www.wcrf.org/int/cancer-facts-figures/data-specific-cancers/colorectal-cancer-statistics.
2. Word Health Organization (2015) Cancer. http://www.who.int/mediacentre/factsheets/fs297/en/.
3. Raskov H, Pommergaard HC, Burcharth J & Rosenberg J (2014) Colorectal carcinogenesis--update and perspectives. *World J Gastroenterol* **20**, 18151-64.
4. Yusof AS, Isa ZM & Shah SA (2012) Dietary patterns and risk of colorectal cancer: a systematic review of cohort studies (2000-2011). *Asian Pac J Cancer Prev* **13**, 4713-7.
5. Bathen TF, Holmgren K, Lundemo AG, Hjelstuen MH, Krokan HE, Gribbestad IS & Schonberg SA (2008) Omega-3 fatty acids suppress growth of SW620 human colon cancer xenografts in nude mice. *Anticancer Res* **28**, 3717-23.
6. Pettersen K, Monsen VT, Hakvag Pettersen CH, Overland HB, Pettersen G, Samdal H, Tesfahun AN, Lundemo AG, Bjorkoy G & Schonberg SA (2016) DHA-induced stress response in human colon cancer cells - Focus on oxidative stress and autophagy. *Free Radic Biol Med* **90**, 158-72.
7. Lee JY, Sim TB, Lee JE & Na HK (2017) Chemopreventive and Chemotherapeutic Effects of Fish Oil derived Omega-3 Polyunsaturated Fatty Acids on Colon Carcinogenesis. *Clinical nutrition research* **6**, 147-160.
8. Hardman WE (2004) (n-3) fatty acids and cancer therapy. *J Nutr* **134**, 3427S-3430S.
9. Skender B, Vaculova AH & Hofmanova J (2012) Docosahexaenoic fatty acid (DHA) in the regulation of colon cell growth and cell death: a review. *Biomed Pap Med Fac Univ Palacky Olomouc Czech Repub* **156**, 186-99.
10. D'Eliseo D & Velotti F (2016) Omega-3 Fatty Acids and Cancer Cell Cytotoxicity: Implications for Multi-Targeted Cancer Therapy. *J Clin Med* **5**.
11. Jakobsen CH, Storvold GL, Bremseth H, Follestad T, Sand K, Mack M, Olsen KS, Lundemo AG, Iversen JG, Krokan HE & Schonberg SA (2008) DHA induces ER stress and growth arrest in human colon cancer cells: associations with cholesterol and calcium homeostasis. *J Lipid Res* **49**, 2089-100.
12. Rashid HO, Yadav RK, Kim HR & Chae HJ (2015) ER stress: Autophagy induction, inhibition and selection. *Autophagy* **11**, 1956-1977.
13. Kania E, Pajak B & Orzechowski A (2015) Calcium homeostasis and ER stress in control of autophagy in cancer cells. *Biomed Res Int* **2015**, 352794.
14. Miyoshi N, Ishii H, Mimori K, Takatsuno Y, Kim H, Hirose H, Sekimoto M, Doki Y & Mori M (2009) Abnormal expression of TRIB3 in colorectal cancer: a novel marker for prognosis. *British journal of cancer* **101**, 1664-70.
15. B'Chir W, Maurin AC, Carraro V, Averous J, Jousse C, Muranishi Y, Parry L, Stepien G, Fafournoux P & Bruhat A (2013) The eIF2alpha/ATF4 pathway is essential for stress-induced autophagy gene expression. *Nucleic Acids Res* **41**, 7683-99.
16. Avivar-Valderas A, Salas E, Bobrovnikova-Marjon E, Diehl JA, Nagi C, Debnath J & Aguirre-Ghiso JA (2011) PERK integrates autophagy and oxidative stress responses to promote survival during extracellular matrix detachment. *Mol Cell Biol* **31**, 3616-29.
17. Mizushima N, Levine B, Cuervo AM & Klionsky DJ (2008) Autophagy fights disease through cellular self-digestion. *Nature* **451**, 1069-75.
18. Mizushima N, Yoshimori T & Levine B (2010) Methods in mammalian autophagy research. *Cell* **140**, 313-26.
19. Rosa A. González-Polo EP-E, Sokhna M. S. Yakhine-Diop, Mario Rodríguez-Arribas, Rubén Gómez-Sánchez, Ignacio Casado-Naranjo, José M. Bravo-San Pedro, José M. Fuentes (2016) The Basics of Autophagy in *Autophagy Networks in Inflammation* (Maria Chiara Maiuri, D. D. S., ed) pp. 3-20, Springer.
20. Bjorkoy G, Lamark T, Brech A, Outzen H, Perander M, Overvatn A, Stenmark H & Johansen T (2005) p62/SQSTM1 forms protein aggregates degraded by autophagy and has a protective effect on huntingtin-induced cell death. *J Cell Biol* **171**, 603-14.

21. Pankiv S, Clausen TH, Lamark T, Brech A, Bruun J-A, Outzen H, Overvatn A, Bjorkoy G & Johansen T (2007) p62/SQSTM1 binds directly to Atg8/LC3 to facilitate degradation of ubiquitinated protein aggregates by autophagy. *J Biol Chem* **282**, 24131-45.
22. Muller PA & Vousden KH (2013) p53 mutations in cancer. *Nat Cell Biol* **15**, 2-8.
23. Muller PA & Vousden KH (2014) Mutant p53 in cancer: new functions and therapeutic opportunities. *Cancer Cell* **25**, 304-17.
24. Tasdemir E, Maiuri MC, Galluzzi L, Vitale I, Djavaheri-Mergny M, D'Amelio M, Criollo A, Morselli E, Zhu C, Harper F, Nannmark U, Samara C, Pinton P, Vicencio JM, Carnuccio R, Moll UM, Madeo F, Paterlini-Brechot P, Rizzuto R, Szabadkai G, Pierron G, Blomgren K, Tavernarakis N, Codogno P, Cecconi F & Kroemer G (2008) Regulation of autophagy by cytoplasmic p53. *Nat Cell Biol* **10**, 676-87.
25. Tang J, Di J, Cao H, Bai J & Zheng J (2015) p53-mediated autophagic regulation: A prospective strategy for cancer therapy. *Cancer Lett* **363**, 101-7.
26. Sui X, Jin L, Huang X, Geng S, He C & Hu X (2011) p53 signaling and autophagy in cancer: a revolutionary strategy could be developed for cancer treatment. *Autophagy* **7**, 565-71.
27. Green DR & Kroemer G (2009) Cytoplasmic functions of the tumour suppressor p53. *Nature* **458**, 1127-30.
28. Huang A, Zhou H, Zhao H, Quan Y, Feng B & Zheng M (2014) TMPRSS4 correlates with colorectal cancer pathological stage and regulates cell proliferation and self-renewal ability. *Cancer biology & therapy* **15**, 297-304.
29. Kontos CK, Papadopoulos IN, Fragoulis EG & Scorilas A (2010) Quantitative expression analysis and prognostic significance of L-DOPA decarboxylase in colorectal adenocarcinoma. *British journal of cancer* **102**, 1384-90.
30. Xu G, Zhang M, Zhu H & Xu J (2017) A 15-gene signature for prediction of colon cancer recurrence and prognosis based on SVM. *Gene* **604**, 33-40.
31. Luo X & Kraus WL (2012) On PAR with PARP: cellular stress signaling through poly(ADP-ribose) and PARP-1. *Genes & development* **26**, 417-32.
32. Kaneko R, Tsuji N, Asanuma K, Tanabe H, Kobayashi D & Watanabe N (2007) Survivin down-regulation plays a crucial role in 3-hydroxy-3-methylglutaryl coenzyme A reductase inhibitor-induced apoptosis in cancer. *J Biol Chem* **282**, 19273-81.
33. Chiu LC & Wan JM (1999) Induction of apoptosis in HL-60 cells by eicosapentaenoic acid (EPA) is associated with downregulation of bcl-2 expression. *Cancer Lett* **145**, 17-27.
34. Farooqi AA, Li KT, Fayyaz S, Chang YT, Ismail M, Liaw CC, Yuan SS, Tang JY & Chang HW (2015) Anticancer drugs for the modulation of endoplasmic reticulum stress and oxidative stress. *Tumour Biol* **36**, 5743-52.
35. Maga G & Hubscher U (2003) Proliferating cell nuclear antigen (PCNA): a dancer with many partners. *J Cell Sci* **116**, 3051-60.
36. Zand H, Rhimipour A, Bakhshayesh M, Shafiee M, Nour Mohammadi I & Salimi S (2007) Involvement of PPAR-gamma and p53 in DHA-induced apoptosis in Reh cells. *Mol Cell Biochem* **304**, 71-7.
37. Shin S, Jing K, Jeong S, Kim N, Song KS, Heo JY, Park JH, Seo KS, Han J, Park JI, Kweon GR, Park SK, Wu T, Hwang BD & Lim K (2013) The omega-3 polyunsaturated fatty acid DHA induces simultaneous apoptosis and autophagy via mitochondrial ROS-mediated Akt-mTOR signaling in prostate cancer cells expressing mutant p53. *Biomed Res Int* **2013**, 568671.
38. Liu Y & Bodmer WF (2006) Analysis of P53 mutations and their expression in 56 colorectal cancer cell lines. *Proc Natl Acad Sci U S A* **103**, 976-81.
39. ATCC COLON CANCER PANELS 1 AND 2. https://www.lgcstandards-atcc.org/~/media/1F2AC21608C54A92901CEFC31D2CB33E.ashx.
40. Kroemer G, Marino G & Levine B (2010) Autophagy and the integrated stress response. *Mol Cell* **40**, 280-93.
41. Medico E, Russo M, Picco G, Cancelliere C, Valtorta E, Corti G, Buscarino M, Isella C, Lamba S, Martinoglio B, Veronese S, Siena S, Sartore-Bianchi A, Beccuti M, Mottolese M, Linnebacher M,

Cordero F, Di Nicolantonio F & Bardelli A (2015) The molecular landscape of colorectal cancer cell lines unveils clinically actionable kinase targets. *Nat Commun* **6**, 7002.
42. Sadanandam A, Lyssiotis CA, Homicsko K, Collisson EA, Gibb WJ, Wullschleger S, Ostos LC, Lannon WA, Grotzinger C, Del Rio M, Lhermitte B, Olshen AB, Wiedenmann B, Cantley LC, Gray JW & Hanahan D (2013) A colorectal cancer classification system that associates cellular phenotype and responses to therapy. *Nat Med* **19**, 619-25.
43. (2016) Somatic mutations - Mutation Prevalence (N=26347). http://p53.iarc.fr/SelectedStatistics.aspx.
44. Jing K, Song KS, Shin S, Kim N, Jeong S, Oh HR, Park JH, Seo KS, Heo JY, Han J, Park JI, Han C, Wu T, Kweon GR, Park SK, Yoon WH, Hwang BD & Lim K (2011) Docosahexaenoic acid induces autophagy through p53/AMPK/mTOR signaling and promotes apoptosis in human cancer cells harboring wild-type p53. *Autophagy* **7**, 1348-58.
45. Xu J, Reumers J, Couceiro JR, De Smet F, Gallardo R, Rudyak S, Cornelis A, Rozenski J, Zwolinska A, Marine J-C, Lambrechts D, Suh Y-A, Rousseau F & Schymkowitz J (2011) Gain of function of mutant p53 by coaggregation with multiple tumor suppressors. *Nat Chem Biol* **7**, 285-95.
46. Kim N, Jeong S, Jing K, Shin S, Kim S, Heo JY, Kweon GR, Park SK, Wu T, Park JI & Lim K (2015) Docosahexaenoic Acid Induces Cell Death in Human Non-Small Cell Lung Cancer Cells by Repressing mTOR via AMPK Activation and PI3K/Akt Inhibition. *Biomed Res Int* **2015**, 239764.
47. Mokarram P, Albokashy M, Zarghooni M, Moosavi MA, Sepehri Z, Chen QM, Hudecki A, Sargazi A, Alizadeh J, Moghadam AR, Hashemi M, Movassagh H, Klonisch T, Owji AA, Los MJ & Ghavami S (2017) New frontiers in the treatment of colorectal cancer: Autophagy and the unfolded protein response as promising targets. *Autophagy*, 1-39.
48. Xiong H-y, Guo X-l, Bu X-x, Zhang S-s, Ma N-n, Song J-r, Hu F, Tao S-f, Sun K, Li R, Wu M-c & Wei L-x (2010) Autophagic cell death induced by 5-FU in Bax or PUMA deficient human colon cancer cell. *Cancer Lett* **288**, 68-74.
49. Li J, Hou N, Faried A, Tsutsumi S & Kuwano H (2010) Inhibition of autophagy augments 5-fluorouracil chemotherapy in human colon cancer in vitro and in vivo model. *Eur J Cancer* **46**, 1900-9.
50. Tan S, Shi H, Ba M, Lin S, Tang H, Zeng X & Zhang X (2016) miR-409-3p sensitizes colon cancer cells to oxaliplatin by inhibiting Beclin-1-mediated autophagy. *Int J Mol Med* **37**, 1030-8.
51. Selvakumaran M, Amaravadi RK, Vasilevskaya IA & O'Dwyer PJ (2013) Autophagy inhibition sensitizes colon cancer cells to antiangiogenic and cytotoxic therapy. *Clin Cancer Res* **19**, 2995-3007.
52. Adams O, Dislich B, Berezowska S, Schlafli AM, Seiler CA, Kroll D, Tschan MP & Langer R (2016) Prognostic relevance of autophagy markers LC3B and p62 in esophageal adenocarcinomas. *Oncotarget* **7**, 39241-39255.
53. Niklaus M, Adams O, Berezowska S, Zlobec I, Graber F, Slotta-Huspenina J, Nitsche U, Rosenberg R, Tschan MP & Langer R (2017) Expression analysis of LC3B and p62 indicates intact activated autophagy is associated with an unfavorable prognosis in colon cancer. *Oncotarget*.
54. Burada F, Nicoli ER, Ciurea ME, Uscatu DC, Ioana M & Gheonea DI (2015) Autophagy in colorectal cancer: An important switch from physiology to pathology. *World J Gastrointest Oncol* **7**, 271-284.
55. Nabavi SF, Bilotto S, Russo GL, Orhan IE, Habtemariam S, Daglia M, Devi KP, Loizzo MR, Tundis R & Nabavi SM (2015) Omega-3 polyunsaturated fatty acids and cancer: lessons learned from clinical trials. *Cancer Metastasis Rev* **34**, 359-80.
56. Gautier L, Cope L, Bolstad BM & Irizarry RA (2004) affy--analysis of Affymetrix GeneChip data at the probe level. *Bioinformatics* **20**, 307-15.
57. Ritchie ME, Phipson B, Wu D, Hu Y, Law CW, Shi W & Smyth GK (2015) limma powers differential expression analyses for RNA-sequencing and microarray studies. *Nucleic Acids Res* **43**, e47.
58. Reimand J, Kull M, Peterson H, Hansen J & Vilo J (2007) g:Profiler--a web-based toolset for functional profiling of gene lists from large-scale experiments. *Nucleic Acids Res* **35**, W193-200.
59. Greene D, Richardson S & Turro E (2017) ontologyX: a suite of R packages for working with ontological data. *Bioinformatics* **33**, 1104-1106.

Table 1. Probes correlating with DHA sensitivity in ten different human CRC cell lines.

Gene symbol	ProbeID	Gene name	Log FC	P value
Autophagy/lysosome/protein metabolism				
AKT3	212609_s_at	V-akt murine thymoma viral oncogene homolog 3	-0.60	0.03
AQP3	203747_at	Aquaporin 3 (Gill blood group)	0.45	0.02
AQP3	39248_at	Aquaporin 3 (Gill blood group)	1.24	0.01
AQP3	39249_at	Aquaporin 3 (Gill blood group)	0.42	0.03
ATP1B1	201242_s_at	ATPase, Na+/K+ transporting, beta 1 polypeptide	1.00	0.01
ATP1B1	201243_s_at	ATPase, Na+/K+ transporting, beta 1 polypeptide	0.91	0.02
CAV1	203065_s_at	Caveolin 1, caveolae protein, 22kDa	-1.55	0.03
CAV1	212097_at	Caveolin 1, caveolae protein, 22kDa	-1.92	0.02
CCDC88A	225045_at	Coiled-coil domain containing 88A	-1.17	0.05
CEACAM6	211657_at	Carcinoembryonic antigen-related cell adhesion molecule 6	2.02	0.02
CEACAM6	203757_s_at	Carcinoembryonic antigen-related cell adhesion molecule 6	1.93	0.03
CTSH	202295_s_at	Cathepsin H	1.43	0.01
DEPTOR	218858_at	DEP domain containing MTOR-interacting protein	1.20	0.00
DYRK2	202971_s_at	Dual-specificity tyrosine-(Y)-phosphorylation regulated kinase 2	0.58	0.05
DYRK2	202969_at	Dual-specificity tyrosine-(Y)-phosphorylation regulated kinase 2	0.45	0.03
FABP1	205892_s_at	Fatty acid binding protein 1, liver	1.90	0.02
FGFR2	203638_s_at	Fibroblast growth factor receptor 2	1.23	0.03
FGFR2	208228_s_at	Fibroblast growth factor receptor 2	1.15	0.05
FZD5	221245_s_at	Frizzled class receptor 5	0.72	0.03
GBA/GBAP1	209093_s_at	Glucosidase, beta, acid/glucosidase, beta, acid pseudogene 1	0.43	0.02
GBAP1	210589_s_at	Glucosidase, beta, acid pseudogene 1	0.45	0.01
LYZ	213975_s_at	Lysozyme	2.96	0.01
LYZ	1555745_a_at	Lysozyme	2.86	0.01
MECOM	226420_at	MDS1 and EVI1 complex locus	2.02	0.00
MECOM	221884_at	MDS1 and EVI1 complex locus	1.72	0.00
MECOM	208434_at	MDS1 and EVI1 complex locus	0.38	0.03
MUC3A/B	217117_x_at	Mucin 3A/B, cell surface associated	0.44	0.02
MUC3A/B	217117_x_at	Mucin 3A/B, cell surface associated	0.44	0.02
P2RX5	210448_s_at	Purinergic receptor P2X, ligand gated ion channel, 5	-1.36	0.00
RAB25	218186_at	RAB25, member RAS oncogene family	1.83	0.04
USP13	226902_at	Ubiquitin specific peptidase 13 (isopeptidase T-3)	-0.59	0.03
Endoplasmic reticulum stress				
AGR2	209173_at	Anterior gradient 2, protein disulphide isomerase family member	2.40	0.03
AGR2	228969_at	Anterior gradient 2, protein disulphide isomerase family member	1.18	0.02
CCND2	200953_s_at	Cyclin D2	2.44	0.04
CCND2	200952_s_at	Cyclin D2	1.37	0.03
CEBPA	204039_at	CCAAT/enhancer binding protein (C/EBP), alpha	0.71	0.01
ERP44	208959_s_at	Endoplasmic reticulum protein 44	0.40	0.03
MLEC	200616_s_at	Malectin	0.83	0.01
MLEC	200617_at	Malectin	0.68	0.01
PDIA5	203857_s_at	Protein disulfide isomerase family A, member 5	0.38	0.02
SERP2	228044_at	Stress-associated endoplasmic reticulum protein family member 2	-0.89	0.05
VIMP	223209_s_at	VCP-interacting membrane selenoprotein	0.32	0.05
Oxidative stress/oxidation-reduction process				
ACOX2	205364_at	Acyl-CoA oxidase 2, branched chain	0.96	0.05
AKR1C3	209160_at	Aldo-keto reductase family 1, member C3	1.41	0.04
ALDH1A1	212224_at	Aldehyde dehydrogenase 1 family, member A1	2.80	0.01
COX4I1	200086_s_at	Cytochrome c oxidase subunit IV isoform 1	0.31	0.04
COX4I1	202698_x_at	Cytochrome c oxidase subunit IV isoform 1	0.27	0.03
COX5B	202343_x_at	Cytochrome c oxidase subunit Vb	0.36	0.04
COX5B	211025_x_at	Cytochrome c oxidase subunit Vb	0.34	0.04
COX5B	213735_s_at	Cytochrome c oxidase subunit Vb	0.32	0.02
CYP4X1	227702_at	Cytochrome P450, family 4, subfamily X, polypeptide 1	1.54	0.02
DECR2	219664_s_at	2,4-dienoyl CoA reductase 2, peroxisomal	0.41	0.02
DEGS2	236496_at	Delta(4)-desaturase, sphingolipid 2	1.16	0.03
ETS1	224833_at	V-ets avian erythroblastosis virus E26 oncogene homolog 1	-1.29	0.02
FADS3	216080_s_at	Fatty acid desaturase 3	-0.61	0.05
HEPH	203903_s_at	Hephaestin	1.93	0.02
HSD17B4	201413_at	Hydroxysteroid (17-beta) dehydrogenase 4	0.57	0.01
MGST2	204168_at	Microsomal glutathione S-transferase 2	0.79	0.00
MSRB2	218773_s_at	Methionine sulfoxide reductase B2	0.60	0.04
NDUFS2	201966_at	NADH dehydrogenase (ubiquinone) Fe-S protein 2, 49kDa	0.34	0.05
NOX1	207217_s_at	NADPH oxidase 1	1.15	0.03
OXR1	223879_s_at	Oxidation resistance 1	-0.85	0.02
OXR1	222553_x_at	Oxidation resistance 1	-0.88	0.02
P3H1	220750_s_at	Prolyl 3-hydroxylase 1	-0.42	0.03
PPARGC1B	232181_at	Peroxisome proliferator-activated receptor gamma, coactivator 1 beta	0.49	0.03
TSTA3	36936_at	Tissue specific transplantation antigen P35B	0.49	0.04
TSTA3	201644_at	Tissue specific transplantation antigen P35B	0.46	0.03

Figure legends

Figure 1

Colorectal cancer cell lines respond differentially to DHA treatment. DHA sensitivity is estimated by cell counting and presented as mean percent of control.

A) DHA sensitivity, measured by cell counting, in ten human colorectal cancer cell lines treated with EtOH or DHA (70 μM) for 48 hours. Results are presented as mean percent of control (±SD), based on three or more independent experiments. *Significantly different from DLD-1 cells (Student's t-test, $p<0.05$).

B) Volcano plot with results from linear regression analyses of log gene expression values for the different probes vs. scaled DHA sensitivity. The x-axis shows the regression slope (logFC from limma) and the y-axis the significance level, which relects how well the gene esxpression fit with the linear model for the scaled DHA sensitivity values. Probes with adjusted p-values <0.05 are color-coded turquoise.

C) Scatter plot of expression levels (x-axis) and scaled DHA sensitivity values (y-axis) for the three most significant probes. Gene and probe names on top of the plots; transmembrane serine protease 4 (TMPRSS4), dopa decarboxylase (DDC) and A-kinase anchoring protein 12 (AKAP12). Dots are cell line expression measurements; blue lines are linear regression fits.

D) Enriched gene ontology terms in the "molecular function" and "cellular compartment" categories for probes with significant positive (Pos Sensitivity; logFC>0 from B) and negative (Neg Sensitivity; logFC<0) correlation to DHA sensitivity levels in the ten cell lines tested. The color-coding reflects level of statistical significance (-log10 adj. p-value), and the size of the circles the odds ratio as calculated by the Fisher's exact test.

E) Enriched gene ontology terms in the "biological process" category for probes with significant positive (Pos Sensitivity; logFC>0 from B) and negative (Neg Sensitivity; logFC<0) correlation to DHA sensitivity levels in the ten cell lines tested. The color coding reflects level of statistical significance (-log10 adj. p-value), and the size of the circles the odds ratio as calculated by the Fisher's exact test.

Figure 2

Effect of DHA treatment on cell growth and the expression of ER stress proteins in DLD-1 and LS411N human CRC cell lines.

A) DHA-induced (70 μM) growth inhibition was measured using cell counting. Results are presented as cell numbers (mean ±SD) from three or more experiments. *Significantly different from control (Student's t-test, $p<0.05$).

B) Changes in level of ER stress-related proteins assessed by western blotting. Results are presented as mean fold change (±SD) from three or more experiments. Band intensities were normalized against the loading control β-actin, and control samples were set to 1 for each time point. Fold change for p-eIF2α and p-PERK represents the ratio to total eIF2a and PERK, respectively. Removal of protein bands representing positive controls on the blots are illustrated by vertical lines. *Significantly different from control (Student's t-test, $p<0.05$).

C) Confocal imaging of ER stress-related proteins after DHA-treatment (70 μM/105 μM) for indicated time periods. Draq5 (blue) was used as nuclear marker. Thapsigargin (TG) was used as positive control. Scale bar 10 μm.

D) The effect of ATF4 knock down (siRNA) on DHA sensitivity in DLD1 cells. Cells were counted (% of control) 24 hours after treatment with DHA (70 μM). Immunoblotting of ATF4 was performed 6 hours after the indicated treatments. NT= Non-target, C= control. *Significantly different from its respective control (Student's t-test, $p<0.05$).

Figure 3

Effect of co-treatment with DHA (70 µM) and the antioxidants BHA (50 µM), BHT (50 µM) and vitamin E (50 µM) on growth of DLD-1 and LS411N cells. Cells were seeded 24 hours prior to co-treatment with DHA and antioxidants. Cells were counted 24 and/or 48 hours after treatment. Results represent the number of cells as % of control (mean ±SD) from three or more experiments, except for vitamin E (DLD-1, n=2). *Significantly different from control (Student's t-test, $p<0.05$). **Significantly different from control and DHA-treated cells (Student's t-test, $p<0.05$).

Figure 4

Effect of DHA-treatment on oxidative stress in CRC cells.

A) Effect of co-treatment with the antioxidant NAC (1 mM) and DHA (70 µM) on growth of DLD-1 and LS411N cells. Cells were treated with DHA 24 hours after seeding alone or in combination with NAC for further 24 and 48 hours. Results represent cell numbers as % of control (mean ±SD) from three or more experiments. *Significantly different from control (Student's t-test, $p<0.05$). **Significantly different from control and DHA-treated cells (Student's t-test, $p<0.05$).

B) The relative level of mitochondrial superoxide (MitoSOX) in DLD-1 and LS411N cells after treatment with DHA (70 µM), NAC (1mM) or a combination of both for 6 and 24 hours. Mitochondrial superoxide was measured by flow cytometry using the fluorescent probe Mitosox. All samples were measured in triplicates. Data represent mean (±SD) fluorescent signal of 10.000 cells from three independent experiments. *Significantly different from control (Student's t-test, $p<0.05$). **Significantly different from control and DHA-treated cells (Student's t-test, $p<0.05$).

C) The relative level of cellular ROS (DCF) in DLD1 and LS411N cells after with DHA (70 µM), NAC (1mM) or a combination of both for 6 and 24 hours. Cellular ROS was measured

by flow cytometry using the fluorescent probe DCF. All samples were measured in triplicates. Data represent mean (±SD) fluorescent signal of 10.000 cells from three independent experiments. *Significantly different from control (Student's t-test, $p<0.05$). **Significantly different from control and DHA-treated cells (Student's t-test, $p<0.05$).
D) The effect of DHA (70 µM) and NAC (1mM) or a combination of both on protein levels of NFE2L2, SQSTM1 and ATF4 at indicated time points. Cox IV was used as loading control. Control samples were set to 1 for each time point. Results represent mean fold change band intensity (±SD) from three experiments. *Significantly different from control (Student's t-test, $p<0.05$). #Significantly different from DHA (Student's t-test, $p<0.05$).

Figure 5

The effect of DHA (70 µM) and NAC (1mM) or a combination of both on TP53 protein level.

A) DLD-1 cells were treated with EtOH, DHA (70 µM), NAC (1 mM), or a combination of both, for 3, 6, 12 and 24 hours. Protein level of TP53 was quantified by immunoblotting. Cox IV was used as loading control. Control samples were set to 1 for each time point. Results represent mean band intensity (±SD) from three experiments. *Significantly different from control (Student's t-test, $p<0.05$). # Significantly different from DHA (Student's t-test, $p<0.05$).

B) Cellular localization of TP53 (green) and MAP1LC3B (red) in DLD-1 cells. DLD-1 cells were treated with EtOH, DHA (70 µM), NAC (1 mM), NAC (1 mM) + DHA (70 µM), BafA1 (100 nM), BafA1 (100 nM) + DHA (70 µM), BafA1 (100 nM) + DHA (70 µM) + NAC (1 mM) or BafA1 (100 nM) + NAC (1 mM), for 24 hours. Protein level and location of TP53 and MAP1LC3B were visualized by confocal imaging. Draq5 (blue) was used as

nuclear marker. Scale bar 20 µm. Numbers on pictures represent percent nuclei positively stained for TP53 (±SD) from three experiments.

C) The effect of knock down of TP53 (siRNA) on cell growth and TP53 protein level in DLD-1 cells. Cell number (% of control) and immunoblotting were performed 48 hours after treatment with EtOH and DHA (70 µM). NT= Non-target, C= control.

Figure 6

Differences in autophagy level between DLD-1 and LS411N cells are important for DHA sensitivity.

A) Protein level and localization of SQSTM1 (green) and MAP1LC3B (red) were visualized by confocal imaging. DLD-1 and LS411N cells were treated with EtOH, DHA (70 µM), NAC (1 mM), NAC (1mM) + DHA (70 µM), BafA1 (100 nM), BafA1 (100 nM) + DHA (70 µM), BafA1 (100 nM) + DHA (70 µM) + NAC (1 mM) or BafA1 (100 nM) + NAC (1 mM), for 12 and 24 hours. Draq5 (blue) was used as nuclear marker. Scale bar 20 µm.

B) Protein level of SQSTM1 and MAP1LC3B-II in DLD1 and LS411N cells treated as specified in Fig 6A. β-actin was used as loading control. Protein levels in control samples and samples treated with BafA1 were set to 1. Vertical lines on the blots illustrate different contrast adjustment of the pictures to visualize the protein bands. *Significantly different from its respective control (Student's t-test, $p<0.05$). **Significantly different from its respective control and DHA-treated cells (Student's t-test, $p<0.05$).

C) The level of autophagic vacuoles assessed by the fluorescent probe Cyto-ID and flow cytometry in DLD-1 and LS411N cells. Cells were treated with EtOH (control), DHA (70 µM), NAC (1 mM), NAC + DHA, BafA1 (100 nM), BafA1 (100 nM) + DHA (70 µM), DMSO, rapamycin (50 nM) and chloroquine (10 µM) for 16 hours. Rapamycin and chloroquine were used as positive and negative control, respectively. DMSO was used as

vehicle for rapamycin. Results are presented as mean fold change (fluorescence/cell, ±SD) from triplicate measurements representing three independent experiments. Cyto ID level in control samples and samples treated with BafA1, were set to 1. *Significantly different from its respective control (Student's t-test, $p<0.05$). **Significantly different from DHA-treated cells (Student's t-test, $p<0.05$).

D) The level of autophagic vacuoles assessed by the fluorescent probe Cyto-ID and flow cytometry in untreated DLD-1 and LS411N cells. Results are presented as mean fluorescence intensity/cell (±SD) from triplicate measurements representing three independent experiments. *Significantly different from LS411N cells (Student's t-test, $p<0.05$).

Figure 7

The basal level of autophagy and MAP1LC3B-II protein level correlate with the degree of DHA sensitivity in CRC cells.

A) Differences in the basal level of autophagy in ten different human CRC cell lines, assessed by flow cytometry using the fluorescent Cyto-ID probe. Results represent mean fold change (±SD) in fluorescence intensity/cell for each cell line, when compared to DLD-1 cells. *Significantly different from DLD-1 cells (Student's t-test, $p<0.05$).

B) Protein level of MAP1LC3B-II in ten CRC cell lines. Band intensities (±SD) are normalized against β-actin as loading control and the MAP1LC3B-II level in LS411N cells was set to 1. *Significantly different from LS411N cells (Student's t-test, $p<0.05$).

C) Graphic illustration of the correlation between log2 transformed basal autophagy level (Cyto-ID) and number of cells (% of control after treatment with DHA (70 μM, 48 h), relative to DLD-1 cells) for ten CRC cell lines.

D) Graphic illustration of the correlation between log2 transformed basal protein level of MAP1LC3B-II and number of cells (% of control after treatment with DHA (70 µM, 48 h), relative to LS411N cells) for ten CRC cell lines.

E) Graphic illustration of the correlation between log2 transformed basal protein level of MAP1LC3B-II and log2 transformed basal autophagy level (relative to LS411N cells) for ten CRC cell lines.

F) The effect of rapamycin treatment on DHA sensitivity and protein level of MAP1LC3B-II in DLD-1 and HCT-8 cells. The cells were treated with EtOH, DHA (70 µM), DMSO, rapamycin (50 nM) and DHA + rapamycin for 48 hours. Results are presented as mean relative cell number (±SD) after cell counting. Relative cell numbers represent the differences in DHA sensitivity after adjusting for the effect of EtOH, DMSO and rapamycin alone. *Significantly different from DHA-treated cells (Student's t-test, $p<0.05$).

Immunoblots represent fold change in band intensities for MAP1LC3B-II after treatment with EtOH, DHA (70 µM), rapamycin (50 nM) and co-treatment with DHA (70 µM) and rapamycin (50 nM) for 24 hours. *Significantly different from control cells (Student's t-test, $p<0.05$). **Significantly different from rapamycin treated cells (Student's t-test, $p<0.05$).

G) The effect of chloroquine treatment on DHA sensitivity and protein level of MAP1LC3B-II in LS411N and LS513 cells. The cells were treated with EtOH, DHA (140 µM), chloroquine (40 and 80 µM) and DHA + chloroquine for 48 h. Results are presented as mean relative cell number (±SD) after cell counting. Mean relative cell numbers (±SD) represent the differences in DHA sensitivity after adjusting for the effect of EtOH and chloroquine alone. *Significantly different from DHA-treated cells (Student's t-test, $p<0.05$).

**Significantly different from cells co-treated with DHA (140 µM) and chloroquine (40 µM) (Student's t-test, $p<0.05$).

Immunoblots represent fold change in band intensities for MAP1LC3B-II after treatement with EtOH, DHA (70 µM), chloroquine (40 µM) and co-treatment with DHA (70 µM) and chloroquine (40 µM) for 24 hours. *Significantly different from control cells (Student's t-test, $p<0.05$). **Significantly different from chloroquine treated cells (Student's t-test, $p<0.05$).

H) The effect of 3-MA treatment on DHA sensitivity and protein level of MAP1LC3B-II in LS411N and LS513 cells. The cells were treated with EtOH, DHA (140 µM), 3-MA (3 mM) and co-treated with DHA (140 µM) and 3-MA (3 mM) for 48 hours. Results are presented as mean relative cell number (±SD) after cell counting. Mean relative cell numbers (±SD) represent the differences in DHA sensitivity after adjusting for the effect of ethanol and 3-MA alone. *Significantly different from DHA-treated cells (Student's t-test, $p<0.05$). Immunoblots represent fold change in band intensities for MAP1LC3B-II after treatment with EtOH, DHA (70 µM), 3-MA (3 mM) and co-treatment with DHA (70 µM) and 3-MA (3 mM) for 24 hours. *Significantly different from control cells (Student's t-test, $p<0.05$). **Significantly different from 3-MA treated cells (Student's t-test, $p<0.05$).

I) The level of autophagic vacuoles assessed by the fluorescent probe Cyto-ID and flow cytometry in DLD-1, HCT-8, LS411N and LS513 cells. DLD-1 and HCT-8 cells were treated with EtOH (control), DHA (70 µM), DMSO (50 nM), rapamycin (50 nM) and co-treatment with rapamycin (50 nM) and DHA (70 µM) for 24 hours. LS411N and LS513 cells were treated with EtOH (control), DHA (70 µM), 3-MA (3 mM) and co-treatment with 3-MA (3 mM) and DHA (70 µM) for 24 hours. Results are presented as mean fold change (fluorescence/cell, ±SD) from triplicate measurements representing three independent experiments. Cyto ID level in control samples and samples treated with DMSO or 3-MA, were set to 1. *Significantly different from its respective control (Student's t-test, $p<0.05$). **Significantly different from cells treated with rapamycin (Student's t-test, $p<0.05$).

Figure 8

Gene expression profiling reveals probes correlating to the level of both DHA sensitivity and basal autophagy in CRC cells. DHA sensitivity is estimated by cell counting and presented as mean percent of control.

A) Correlation of probes to scaled DHA sensitivity values (x-axis) and scaled basal autophagy values (y-axis). The values along the axes represent the slope for the corresponding linear regression (logFC from limma). One dot represents one probe, and is color coded with respect to statistically significant correlation to basal autophagy level (green), DHA sensitivity (purple), and both basal autophagy levels and DHA sensitivity levels (orange). Non-significant probes are shown in gray.

B) Correlation of probes after accounting for residuals in the analysis. Axes and color coding as in Fig. 8A.

C) Selected enriched GO terms for probes with significant positive (Pos) or negative (Neg) correlation to basal autophagy or DHA sensitivity levels in the ten cell lines tested, in addition to the probes significant in the analyses including residuals (denoted R). The color-coding reflects level of statistical significance (-log10 adj. p-value), and the size of the circles the odds ratio as calculated by Fisher's exact test.

D) The most significantly enriched GO terms in the cellular compartment category. Axes, color and size coding as in Fig. 8C.

E) Expression values of gene probes with known functions in autophagy compared to the scaled value for basal autophagy level (bottom panel) and DHA sensitivity (top panel) for the ten cell lines. The probes were all significantly correlated to the basal autophagy and DHA sensitivity levels in the cell lines. Significant correlation is denoted with turquoise.

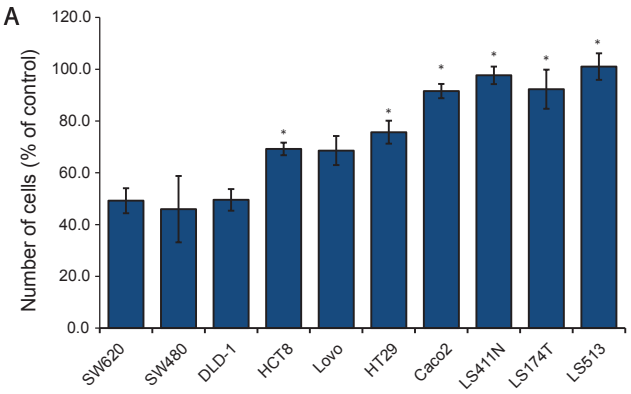
A
Number of cells (% of control)
120.0
100.0
80.0
60.0
40.0
20.0
0.0
SW620
SW480
DLD-1
HCT8
Lovo
HT29
Caco2
LS411N
LS174T
LS513

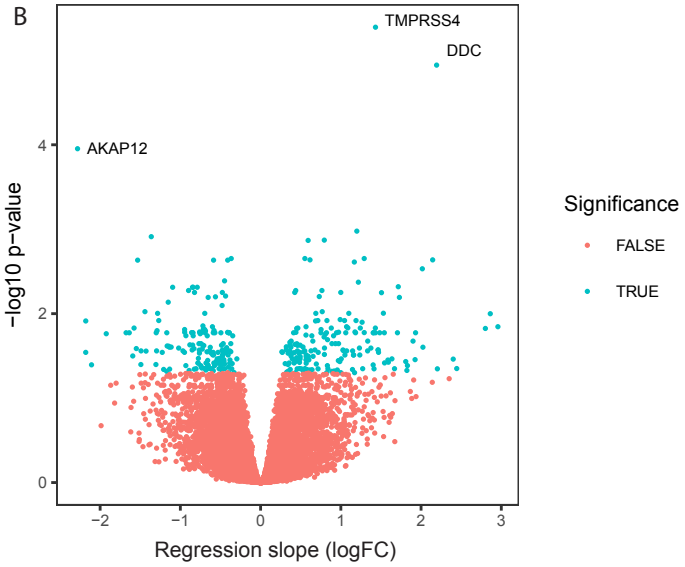
B
TMPRSS4
DDC
AKAP12
−log10 p−value
Regression slope (logFC)
Significance
FALSE
TRUE

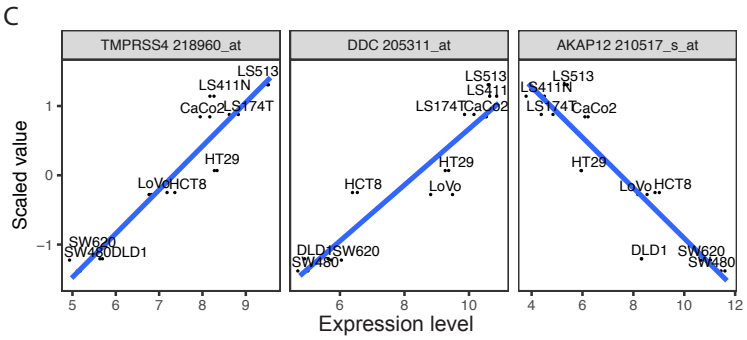
C
TMPRSS4 218960_at
DDC 205311_at
AKAP12 210517_s_at
Scaled value
Expression level

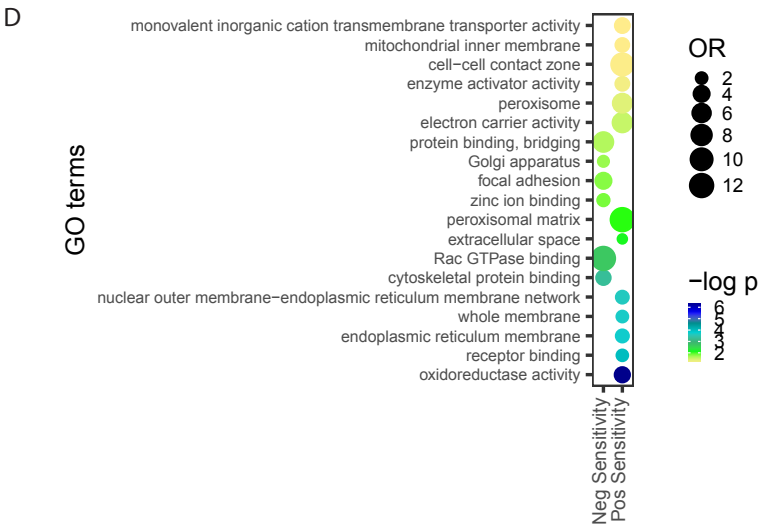
D
monovalent inorganic cation transmembrane transporter activity
mitochondrial inner membrane
cell−cell contact zone
enzyme activator activity
peroxisome
electron carrier activity
protein binding, bridging
Golgi apparatus
focal adhesion
zinc ion binding
peroxisomal matrix
extracellular space
Rac GTPase binding
cytoskeletal protein binding
nuclear outer membrane−endoplasmic reticulum membrane network
whole membrane
endoplasmic reticulum membrane
receptor binding
oxidoreductase activity
GO terms
Neg Sensitivity
Pos Sensitivity
OR
−log p

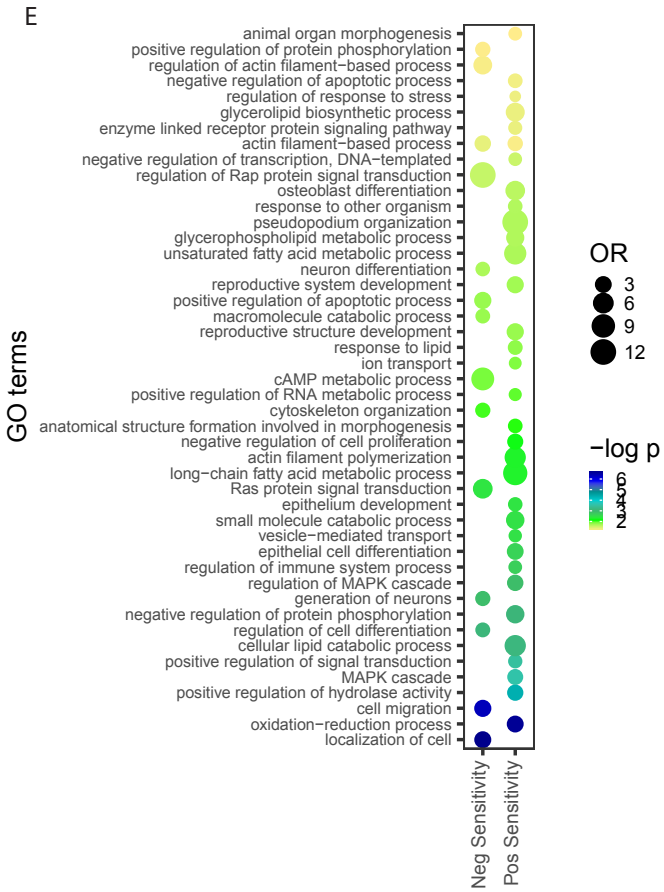
E
animal organ morphogenesis
positive regulation of protein phosphorylation
regulation of actin filament−based process
negative regulation of apoptotic process
regulation of response to stress
glycerolipid biosynthetic process
enzyme linked receptor protein signaling pathway
actin filament−based process
negative regulation of transcription, DNA−templated
regulation of Rap protein signal transduction
osteoblast differentiation
response to other organism
pseudopodium organization
glycerophospholipid metabolic process
unsaturated fatty acid metabolic process
neuron differentiation
reproductive system development
positive regulation of apoptotic process
macromolecule catabolic process
reproductive structure development
response to lipid
ion transport
cAMP metabolic process
positive regulation of RNA metabolic process
cytoskeleton organization
anatomical structure formation involved in morphogenesis
negative regulation of cell proliferation
actin filament polymerization
long−chain fatty acid metabolic process
Ras protein signal transduction
epithelium development
small molecule catabolic process
vesicle−mediated transport
epithelial cell differentiation
regulation of immune system process
regulation of MAPK cascade
generation of neurons
negative regulation of protein phosphorylation
regulation of cell differentiation
cellular lipid catabolic process
positive regulation of signal transduction
MAPK cascade
positive regulation of hydrolase activity
cell migration
oxidation−reduction process
localization of cell
GO terms
Neg Sensitivity
Pos Sensitivity
OR
−log p

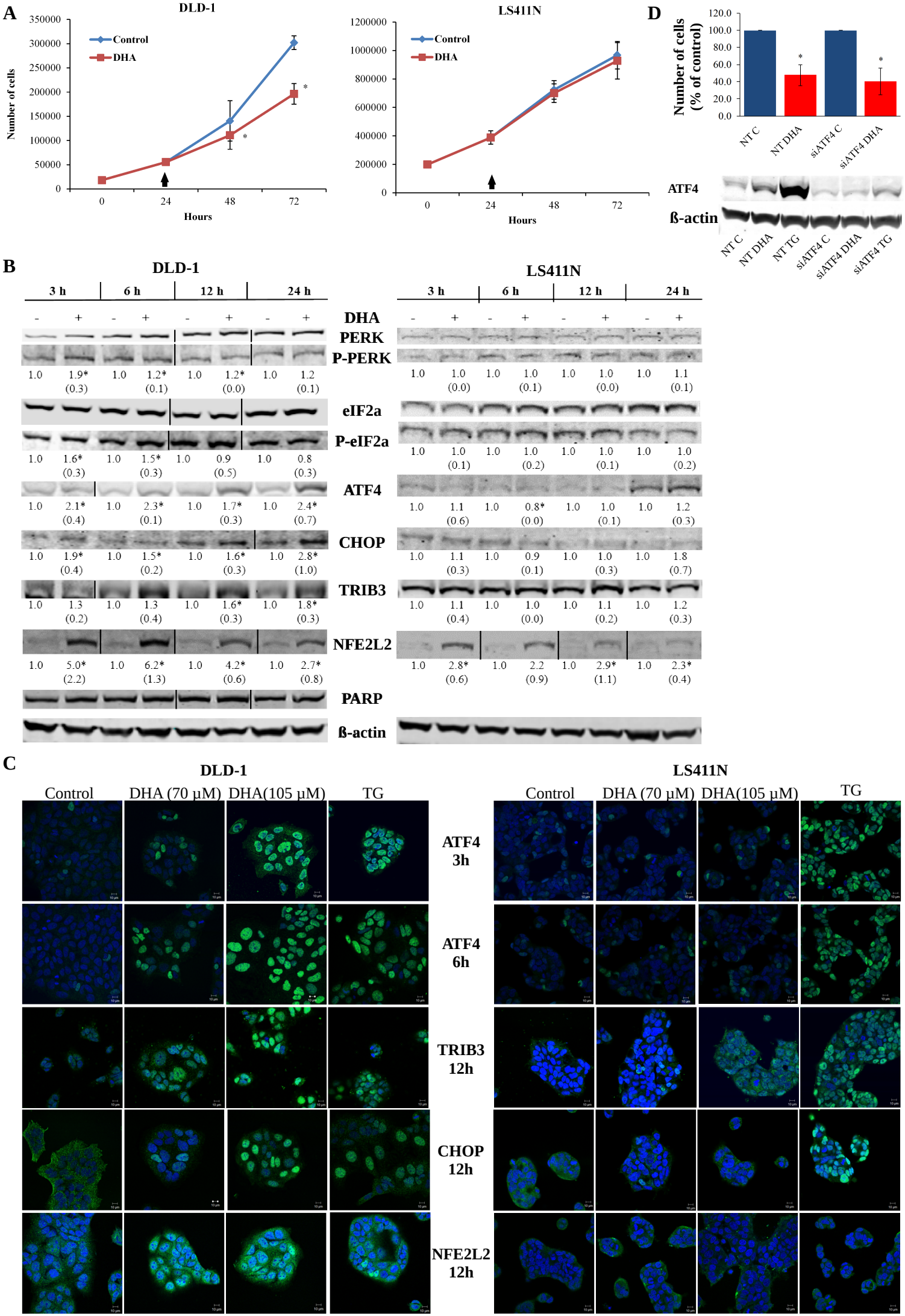
A
DLD-1
Control
DHA
Number of cells
Hours
LS411N
Control
DHA
Hours
D
Number of cells (% of control)
NT C
NT DHA
siATF4 C
siATF4 DHA
ATF4
ß-actin
NT C
NT DHA
NT TG
siATF4 C
siATF4 DHA
siATF4 TG
B
DLD-1
LS411N
3 h
6 h
12 h
24 h
DHA
PERK
P-PERK
eIF2a
P-eIF2a
ATF4
CHOP
TRIB3
NFE2L2
PARP
ß-actin
C
DLD-1
LS411N
Control
DHA (70 µM)
DHA(105 µM)
TG
ATF4 3h
ATF4 6h
TRIB3 12h
CHOP 12h
NFE2L2 12h

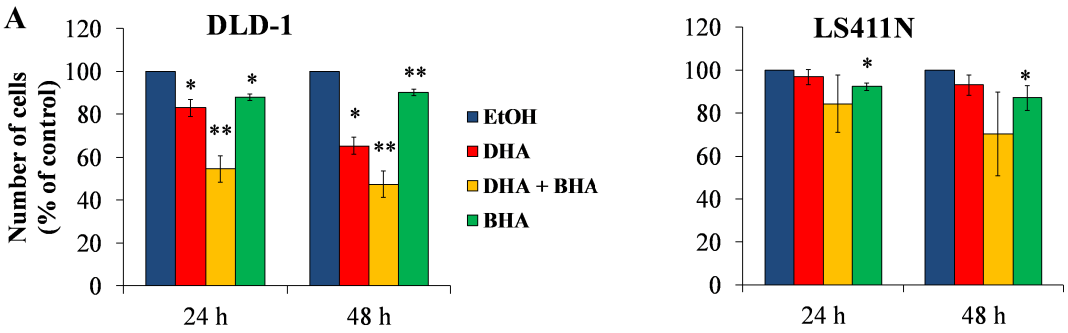
A
DLD-1
LS411N
Number of cells (% of control)
120
100
80
60
40
20
0
24 h
48 h
EtOH
DHA
DHA + BHA
BHA
*
**

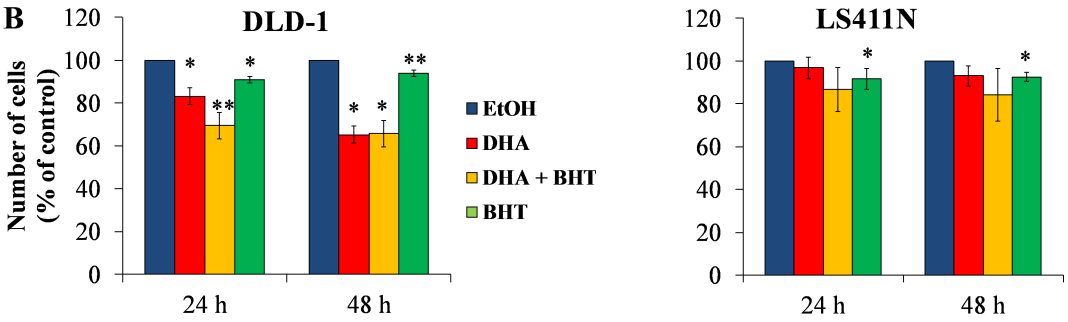
B
DLD-1
LS411N
Number of cells (% of control)
120
100
80
60
40
20
0
24 h
48 h
EtOH
DHA
DHA + BHT
BHT
*
**

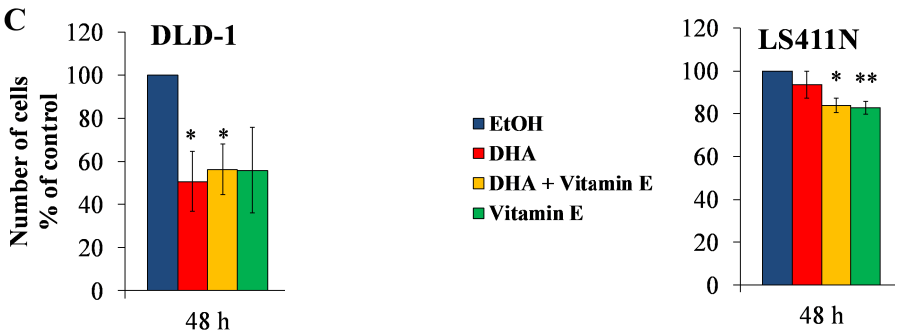
C
DLD-1
LS411N
Number of cells % of control
120
100
80
60
40
20
0
48 h
EtOH
DHA
DHA + Vitamin E
Vitamin E
*
**

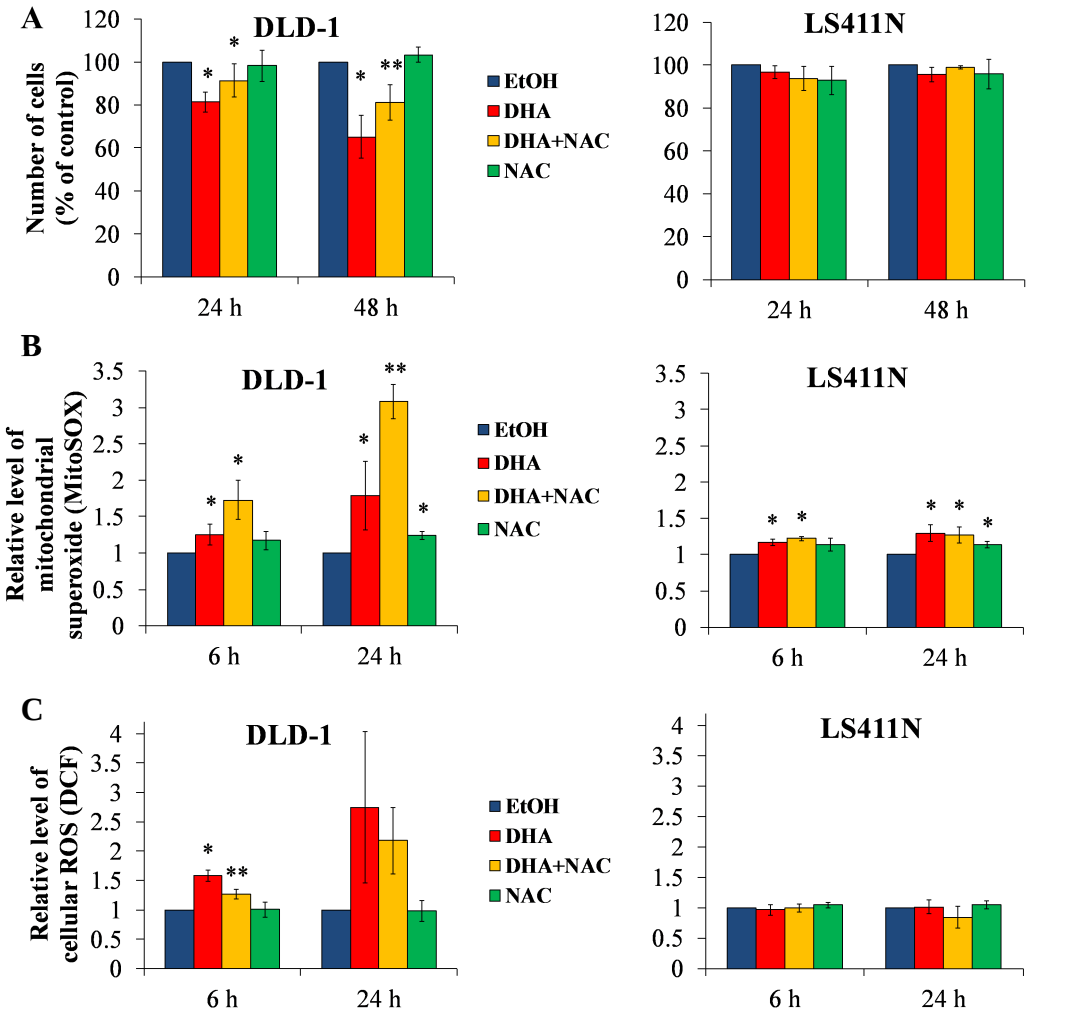
A
DLD-1
LS411N
Number of cells (% of control)
EtOH
DHA
DHA+NAC
NAC
24 h
48 h
B
Relative level of mitochondrial superoxide (MitoSOX)
6 h
24 h
C
Relative level of cellular ROS (DCF)

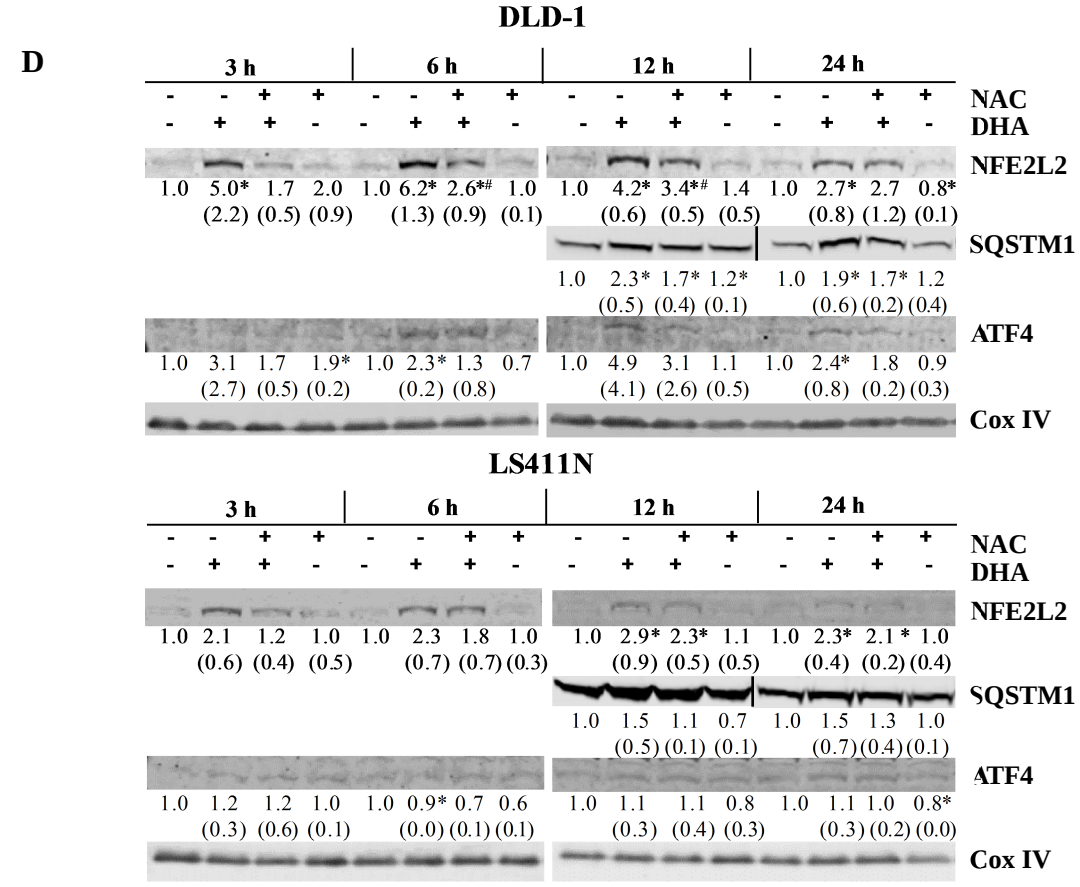
D
DLD-1
3 h
6 h
12 h
24 h
NAC
DHA
NFE2L2
1.0 5.0* 1.7 2.0 1.0 6.2* 2.6*# 1.0 1.0 4.2* 3.4*# 1.4 1.0 2.7* 2.7 0.8*
(2.2) (0.5) (0.9) (1.3) (0.9) (0.1) (0.6) (0.5) (0.5) (0.8) (1.2) (0.1)
SQSTM1
1.0 2.3* 1.7* 1.2* 1.0 1.9* 1.7* 1.2
(0.5) (0.4) (0.1) (0.6) (0.2) (0.4)
ATF4
1.0 3.1 1.7 1.9* 1.0 2.3* 1.3 0.7 1.0 4.9 3.1 1.1 1.0 2.4* 1.8 0.9
(2.7) (0.5) (0.2) (0.2) (0.8) (4.1) (2.6) (0.5) (0.8) (0.2) (0.3)
Cox IV
LS411N
1.0 2.1 1.2 1.0 1.0 2.3 1.8 1.0 1.0 2.9* 2.3* 1.1 1.0 2.3* 2.1 * 1.0
(0.6) (0.4) (0.5) (0.7) (0.7) (0.3) (0.9) (0.5) (0.5) (0.4) (0.2) (0.4)
1.0 1.5 1.1 0.7 1.0 1.5 1.3 1.0
(0.5) (0.1) (0.1) (0.7) (0.4) (0.1)
1.0 1.2 1.2 1.0 1.0 0.9* 0.7 0.6 1.0 1.1 1.1 0.8 1.0 1.1 1.0 0.8*
(0.3) (0.6) (0.1) (0.0) (0.1) (0.1) (0.3) (0.4) (0.3) (0.3) (0.2) (0.0)

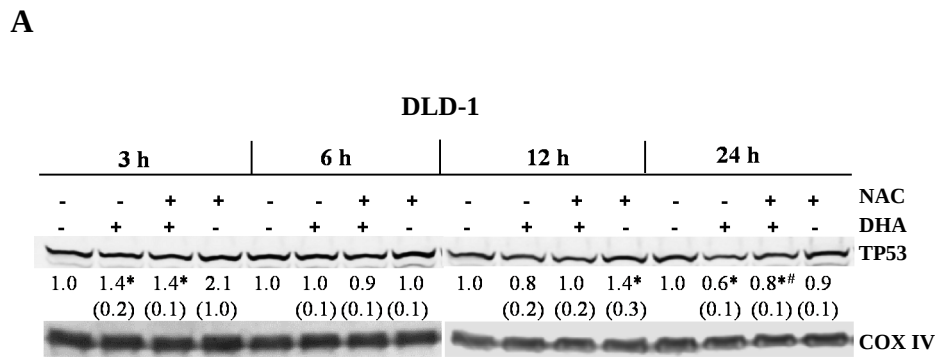

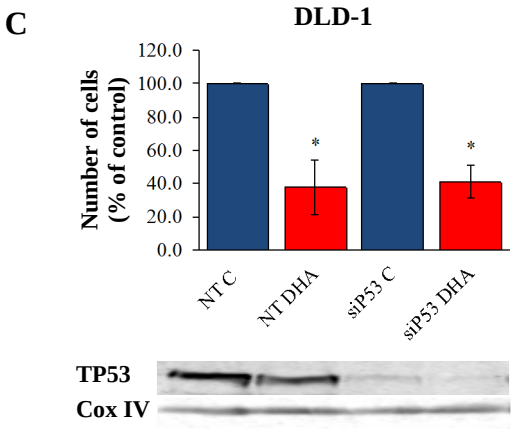

B **DLD-1 24 h** (TP53 = green, LC3B = red)

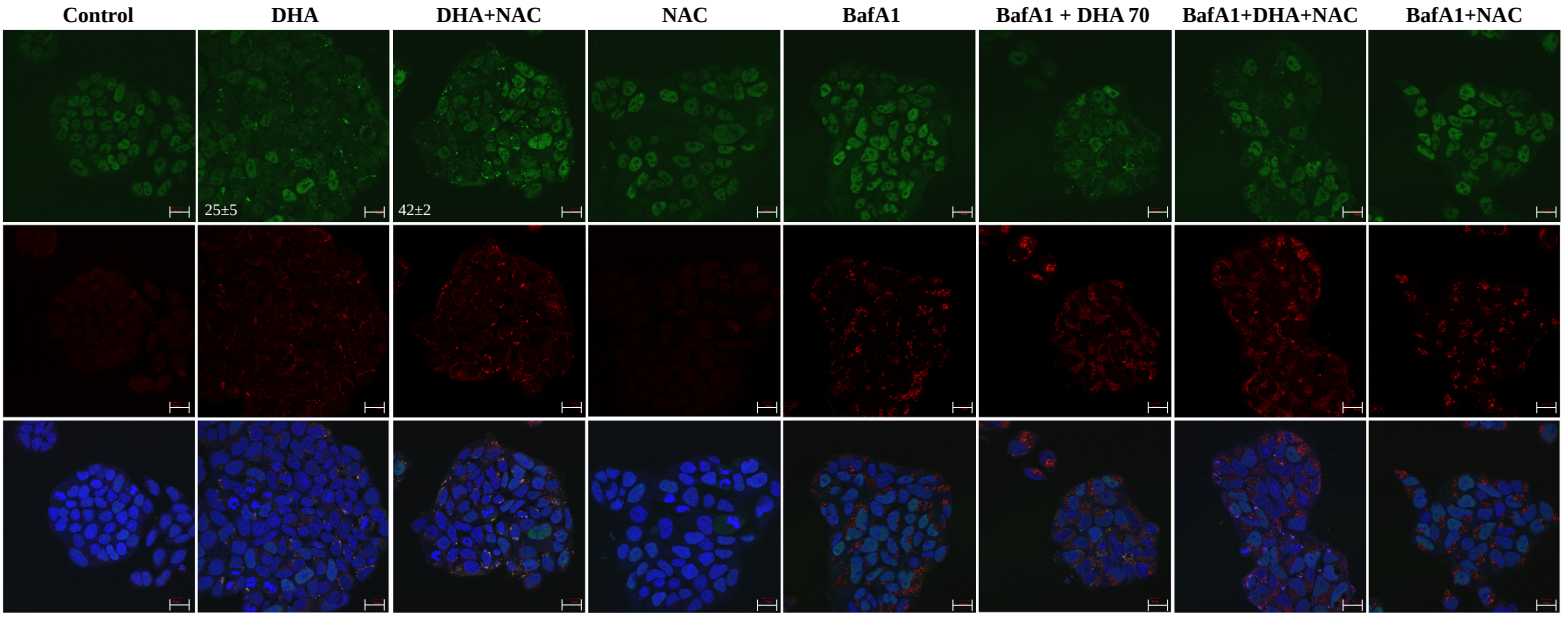

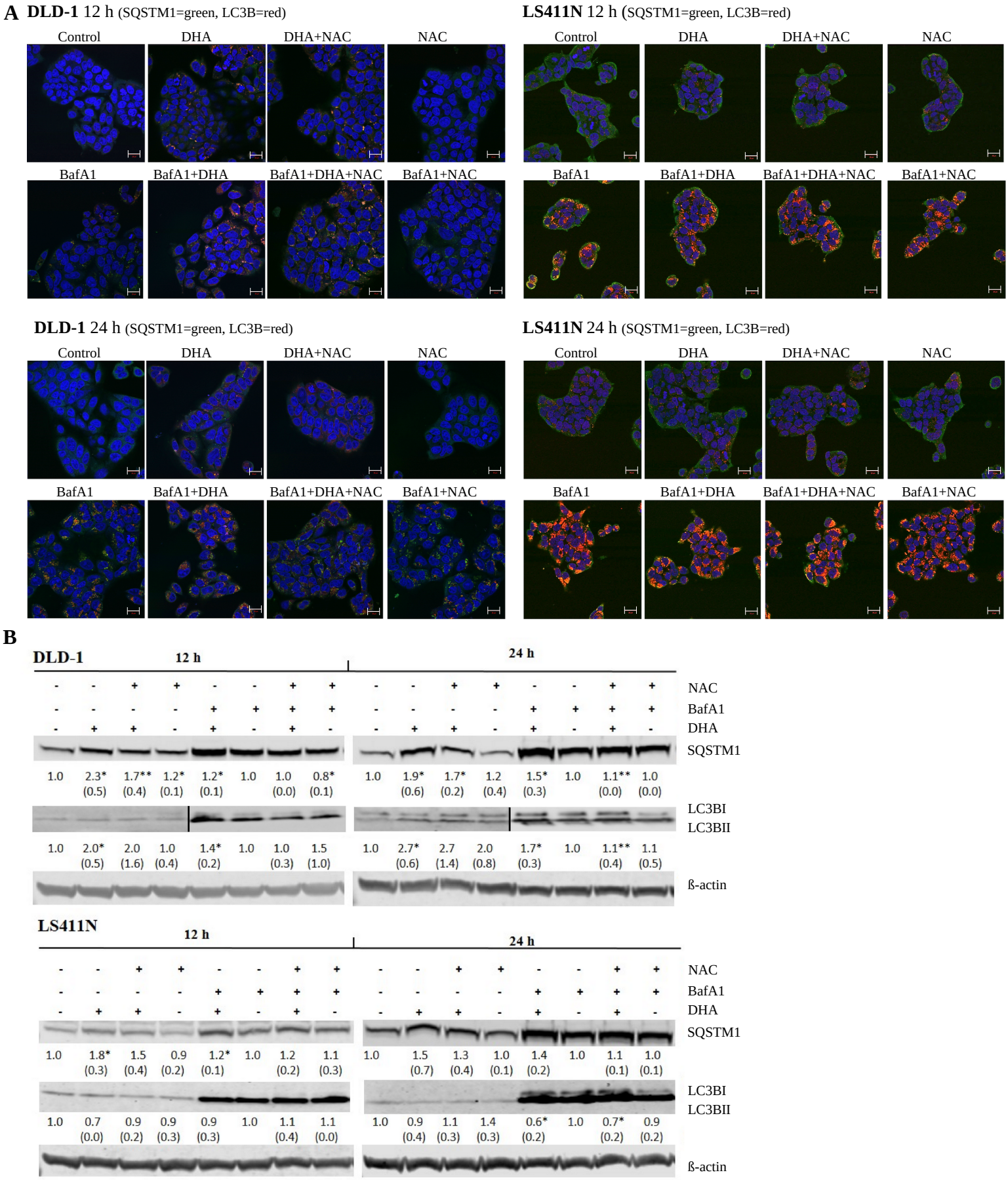
A
DLD-1 12 h (SQSTM1=green, LC3B=red)
LS411N 12 h (SQSTM1=green, LC3B=red)
Control
DHA
DHA+NAC
NAC
BafA1
BafA1+DHA
BafA1+DHA+NAC
BafA1+NAC
DLD-1 24 h (SQSTM1=green, LC3B=red)
LS411N 24 h (SQSTM1=green, LC3B=red)
B
DLD-1
12 h
24 h
NAC
BafA1
DHA
SQSTM1
1.0 2.3* (0.5) 1.7** (0.4) 1.2* (0.1) 1.2* (0.1) 1.0 1.0 (0.0) 0.8* (0.1)
1.0 1.9* (0.6) 1.7* (0.2) 1.2 (0.4) 1.5* (0.3) 1.0 1.1** (0.0) 1.0 (0.0)
LC3BI
LC3BII
1.0 2.0* (0.5) 2.0 (1.6) 1.0 (0.4) 1.4* (0.2) 1.0 1.0 (0.3) 1.5 (1.0)
1.0 2.7* (0.6) 2.7 (1.4) 2.0 (0.8) 1.7* (0.3) 1.0 1.1** (0.4) 1.1 (0.5)
ß-actin
LS411N
12 h
24 h
1.0 1.8* (0.3) 1.5 (0.4) 0.9 (0.2) 1.2* (0.1) 1.0 1.2 (0.2) 1.1 (0.3)
1.0 1.5 (0.7) 1.3 (0.4) 1.0 (0.1) 1.4 (0.2) 1.0 1.1 (0.1) 1.0 (0.1)
1.0 0.7 (0.0) 0.9 (0.2) 0.9 (0.3) 0.9 (0.3) 1.0 1.1 (0.4) 1.1 (0.0)
1.0 0.9 (0.4) 1.1 (0.3) 1.4 (0.3) 0.6* (0.2) 1.0 0.7* (0.2) 0.9 (0.2)
C
DLD-1
LS411N
Cyto ID
Fold change (fluorescence/cell)
Control
DHA
NAC
NAC + DHA
BafA1
BafA1 + DHA
DMSO
Rapamycin
Chloroquine
D
Cyto-ID
Mean Fluorescence Intensity/cell
p=0.003
DLD-1
LS411N

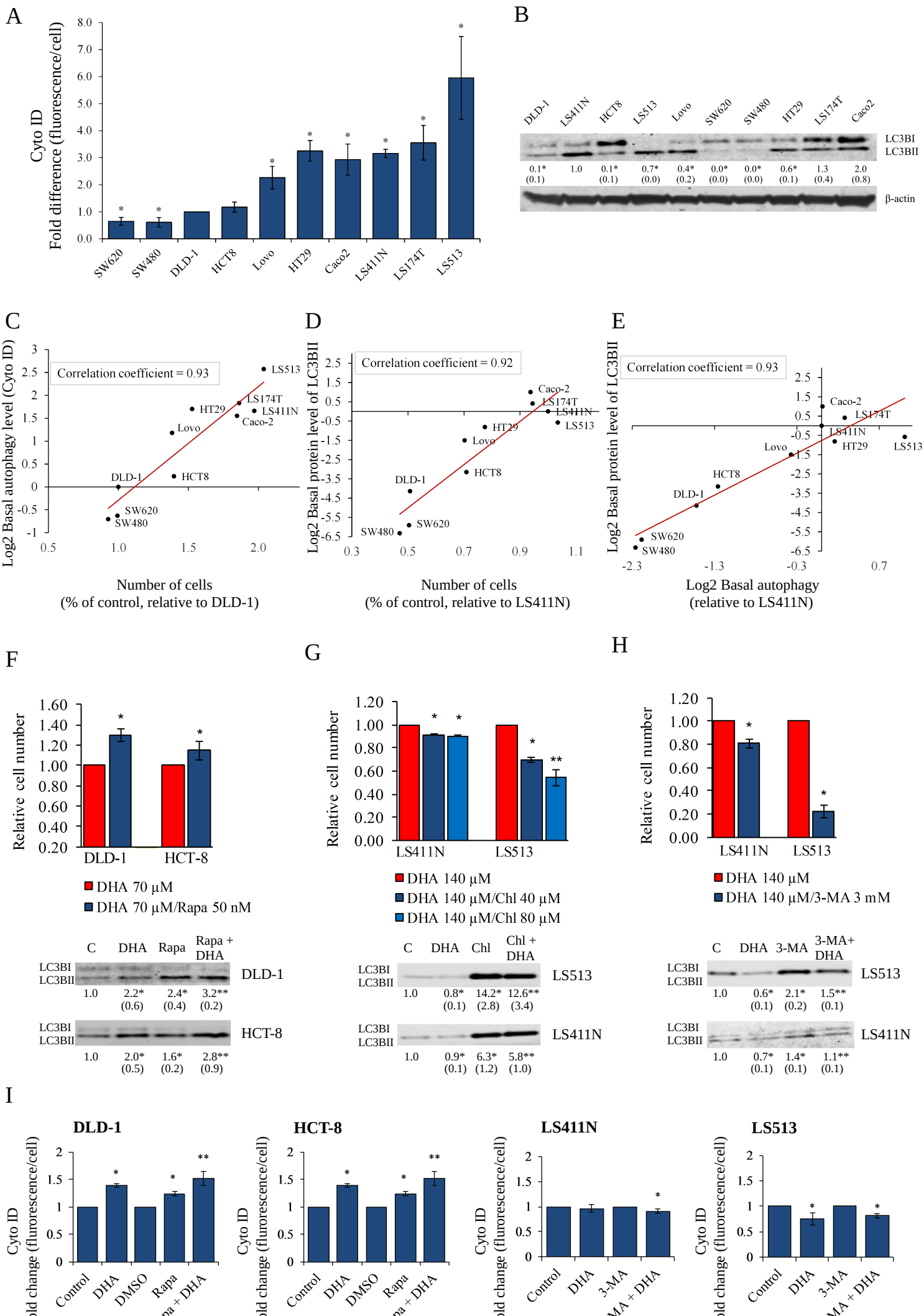
A
Cyto ID
Fold difference (fluorescence/cell)
SW620
SW480
DLD-1
HCT8
Lovo
HT29
Caco2
LS411N
LS174T
LS513
B
DLD-1
LS411N
HCT8
LS513
Lovo
SW620
SW480
HT29
LS174T
Caco2
LC3BI
LC3BII
β-actin
C
Log2 Basal autophagy level (Cyto ID)
Correlation coefficient = 0.93
Number of cells
(% of control, relative to DLD-1)
D
Log2 Basal protein level of LC3BII
Correlation coefficient = 0.92
Number of cells
(% of control, relative to LS411N)
E
Log2 Basal protein level of LC3BII
Correlation coefficient = 0.93
Log2 Basal autophagy
(relative to LS411N)
F
Relative cell number
DLD-1
HCT-8
DHA 70 μM
DHA 70 μM/Rapa 50 nM
C
DHA
Rapa
Rapa + DHA
G
Relative cell number
LS411N
LS513
DHA 140 μM
DHA 140 μM/Chl 40 μM
DHA 140 μM/Chl 80 μM
Chl
Chl + DHA
H
Relative cell number
DHA 140 μM
DHA 140 μM/3-MA 3 mM
3-MA
3-MA+ DHA
I
DLD-1
HCT-8
LS411N
LS513
Cyto ID
Fold change (fluorescence/cell)
Control
DHA
DMSO
Rapa
Rapa + DHA
3-MA
3-MA + DHA

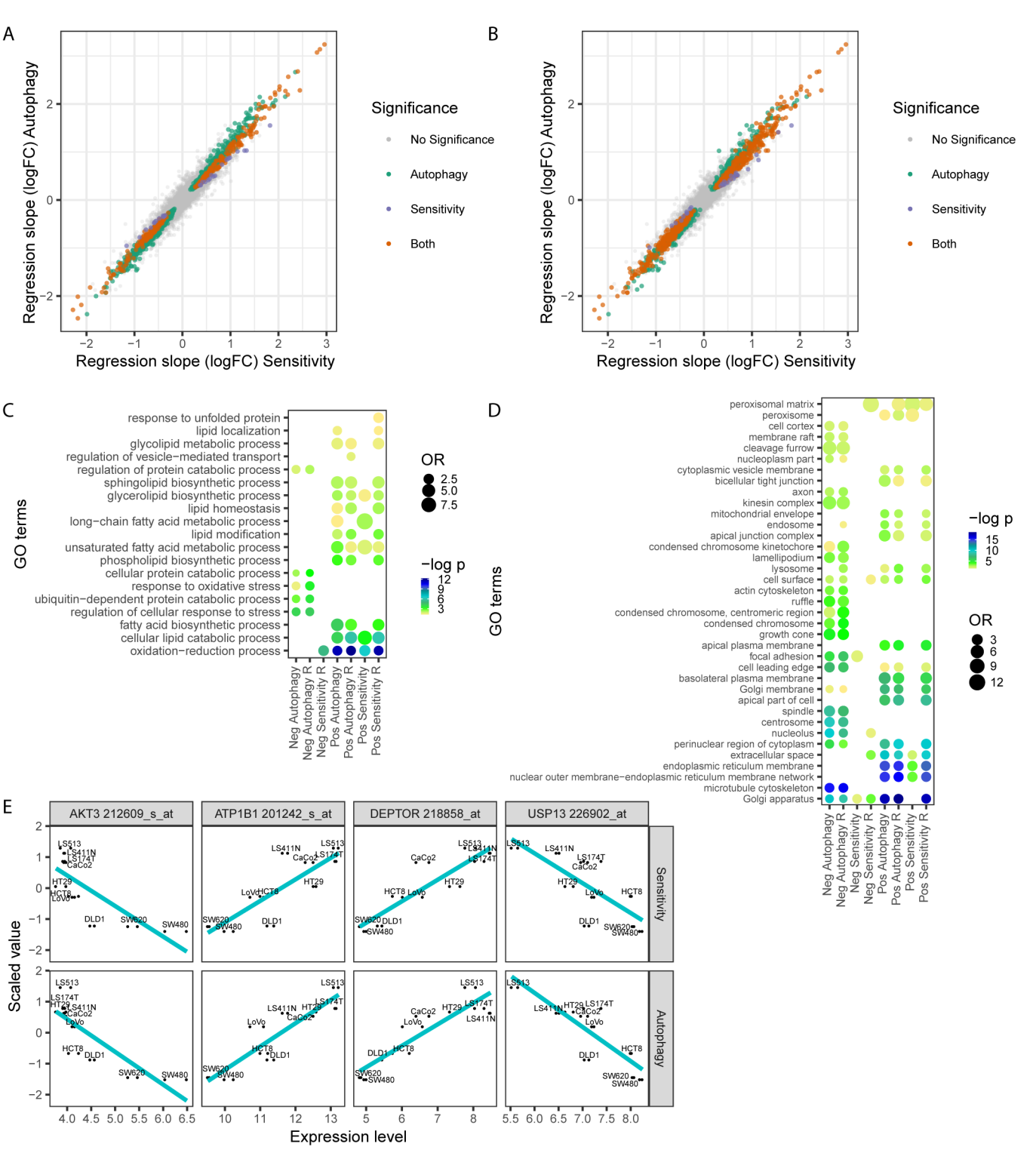
A
Regression slope (logFC) Autophagy
Regression slope (logFC) Sensitivity
Significance
No Significance
Autophagy
Sensitivity
Both
B
Regression slope (logFC) Autophagy
Regression slope (logFC) Sensitivity
Significance
No Significance
Autophagy
Sensitivity
Both
C
GO terms
response to unfolded protein
lipid localization
glycolipid metabolic process
regulation of vesicle−mediated transport
regulation of protein catabolic process
sphingolipid biosynthetic process
glycerolipid biosynthetic process
lipid homeostasis
long−chain fatty acid metabolic process
lipid modification
unsaturated fatty acid metabolic process
phospholipid biosynthetic process
cellular protein catabolic process
response to oxidative stress
ubiquitin−dependent protein catabolic process
regulation of cellular response to stress
fatty acid biosynthetic process
cellular lipid catabolic process
oxidation−reduction process
Neg Autophagy
Neg Autophagy R
Neg Sensitivity R
Pos Autophagy
Pos Autophagy R
Pos Sensitivity
Pos Sensitivity R
OR
2.5
5.0
7.5
−log p
12
9
6
3
D
GO terms
peroxisomal matrix
peroxisome
cell cortex
membrane raft
cleavage furrow
nucleoplasm part
cytoplasmic vesicle membrane
bicellular tight junction
axon
kinesin complex
mitochondrial envelope
endosome
apical junction complex
condensed chromosome kinetochore
lamellipodium
lysosome
cell surface
actin cytoskeleton
ruffle
condensed chromosome, centromeric region
condensed chromosome
growth cone
apical plasma membrane
focal adhesion
cell leading edge
basolateral plasma membrane
Golgi membrane
apical part of cell
spindle
centrosome
nucleolus
perinuclear region of cytoplasm
extracellular space
endoplasmic reticulum membrane
nuclear outer membrane−endoplasmic reticulum membrane network
microtubule cytoskeleton
Golgi apparatus
Neg Autophagy
Neg Autophagy R
Neg Sensitivity R
Pos Autophagy
Pos Autophagy R
Pos Sensitivity
Pos Sensitivity R
−log p
15
10
5
OR
3
6
9
12
E
AKT3 212609_s_at
ATP1B1 201242_s_at
DEPTOR 218858_at
USP13 226902_at
Sensitivity
Autophagy
Scaled value
Expression level
LS513
LS411N
LS174T
CaCo2
HT29
HCT8
LoVo
DLD1
SW620
SW480